TURUN
YLIOPISTO
UNIVERSITY
OF TURKU

Image analysis of stetaotic liver disease in preclinical mouse models

Defining the role of HSD17B12 in lipid homeostasis

Laura Mairinoja

TURUN YLIOPISTON JULKAISUJA – ANNALES UNIVERSITATIS TURKUENSIS
SARJA - SER. D OSA - TOM. 1935 | MEDICA – ODONTOLOGICA | TURKU 2025

TURUN
YLIOPISTO
UNIVERSITY
OF TURKU

IMAGE ANALYSIS OF STETAOTIC LIVER DISEASE IN PRECLINICAL MOUSE MODELS

Defining the role of HSD17B12 in lipid homeostasis

Laura Mairinoja

TURUN YLIOPISTON JULKAISUJA – ANNALES UNIVERSITATIS TURKUENSIS
SARJA – SER. D OSA – TOM. 1935 | MEDICA – ODONTOLOGICA | TURKU 2025

University of Turku

Faculty of Medicine
Institute of Biomedicine
Physiology
Drug Research Doctoral Programme

Supervised by

Professor Matti Poutanen, PhD
Faculty of Medicine
Institute of Biomedicine
Research Centre for Integrative Physiology and Pharmacology
University of Turku
Turku, Finland

Docent Leena Strauss, PhD
Faculty of Medicine
Institute of Biomedicine
Research Centre for Integrative Physiology and Pharmacology
University of Turku
Turku, Finland

Associate Professor Pekka Ruusuvuori, PhD
Faculty of Medicine
Institute of Biomedicine
Cancer Research Unit
University of Turku
Turku, Finland

Reviewed by

Docent Veli-Pekka Ronkainen, PhD
Biocenter Oulu
University of Oulu
Oulu, Finland

Professor Alex Odermatt, PhD
Departement Pharmazeutische Wissenschaften
University of Basel
Basel, Schweiz

Opponent

Associate Professor Panu K. Luukkonen, MD, PhD
Institute for Molecular Medicine Finland, Helsinki Institute of Life Sciences and Department of Internal Medicine, Faculty of Medicine, University of Helsinki;
Transplantation and Liver Surgery, Abdominal Center, Helsinki University Hospital;
Minerva Foundation Institute for Medical Research
Helsinki, Finland

Cover Image: Laura Mairinoja and Joanna Pylvänäinen

ISBN 978-952-02-0473-0 (PRINT)
ISBN 978-952-02-0474-7 (PDF)
ISSN 0355-9483 (Print)
ISSN 2343-3213 (Online)
Painosalama, Turku, Finland 2025

To the memory of my beloved mother,
who will always inspire me.

UNIVERSITY OF TURKU
Faculty of Medicine
Institute of Biomedicine
Physiology
LAURA MAIRINOJA: Image analysis of steatotic liver disease in preclinical mouse models - Defining the role of HSD17B12 in lipid homeostasis
Doctoral Dissertation, 126 pp.
Drug Research Doctoral Programme
December 2025

ABSTRACT

Metabolic dysfunction-associated steatotic liver disease (MASLD), formerly known as non-alcoholic fatty liver disease (NAFLD), and its progressive form, metabolic dysfunction-associated steatohepatitis (MASH), are liver manifestations of the metabolic syndrome. Their global prevalence is rising alongside obesity, highlighting the need for new therapeutic targets. In this work, a deep learning-based image analysis model was developed to quantify liver steatosis in histological whole-slide images of preclinical MASLD models. The algorithm accurately identifies parenchymal tissue while excluding background, fixation artifacts, and vessels, then detects and quantifies regions with microvesicular and macrovesicular steatosis. This approach was applied to study the role of HSD17B12 in the development of steatotic liver disease using mice with a hepatocyte-specific knockout of HSD17B12 (LiB12cKO). On a chow diet, these mice exhibited hepatic lipid accumulation with reduced whole-body fat, characterized predominantly by microvesicular steatosis, indicating impaired lipid droplet expansion. These changes were associated with hepatocellular hypertrophy and hepatic injury. A high-fat diet intervention was implemented, and subsequent morphological and functional alterations were evaluated using histological image analysis, transmission electron microscopy, and micro-ultrasound imaging. Notably, LiB12cKO mice were resistant to high-fat diet–induced obesity and hepatic steatosis, as demonstrated by image analysis and complementary biomarkers. Transcriptomic profiling further supported these findings, revealing significant changes in LiB12cKO males compared to wild-type controls. Taken together, these results suggest that inactivation of HSD17B12 alters liver morphology and lipid metabolism, but offers a potential approach to reduce diet-induced obesity.

KEYWORDS: Image analysis, mouse model, HSD17B12, metabolic dysfunction-associated steatotic liver disease, MASLD

TURUN YLIOPISTO
Lääketieteellinen tiedekunta
Biolääketieteen laitos
Fysiologia
LAURA MAIRINOJA: Rasvamaksasairauden kuva-analyysit prekliinisissä hiirimalleissa - HSD17B12 entsyymin rooli rasva-aineenvaihdunnassa
Väitöskirja, 126 s.
Lääketutkimuksen tohtoriohjelma
Joulukuu 2025

TIIVISTELMÄ

Metabolinen rasvamaksatauti (metabolic dysfunction-associated steatotic liver disease, MASLD) ja sen agressiivisempi tautimuoto, steatohepatiitti eli rasvamaksatulehdus (metabolic dysfunction associated steatohepatitis, MASH) ovat monimutkaisia sairauksia, joihin liittyy aineenvaihduntahäiriöitä. Nämä sairaudet lisääntyvät jatkuvasti maailmanlaajuisesti ylipainon lisääntymisen myötä, mikä korostaa uusien hoitomuotojen kehittämisen tärkeyttä. Tässä väitöskirjatyössä kehitettiin syväoppimiseen perustuva kuva-analyysimalli, joka havaitsee ja mittaa maksan rasvoittumista MASLD-hiirimallien histologisista kuvista. Algoritmi tunnistaa tarkasti maksakudoksen ja sulkee pois taustan, artefaktit ja verisuonet, minkä jälkeen se havaitsee ja mittaa mikrovesikulaarisen ja makrovesikulaarisen rasvoittumisen alueet. Kehitettyä menetelmää hyödynnettiin HSD17B12-entsyymin roolin tutkimiseksi rasvamaksataudin kehittymisessä hiirimallilla, jossa HSD17B12:n toiminta on estetty maksasoluissa (LiB12cKO). Perusruokavaliolla (chow) LiB12cKO-hiirillä havaittiin merkittävää rasvan kertymistä maksaan sekä koko kehon rasvapitoisuuden vähenemistä. Histologisesti maksan rasvoittuminen oli pääasiassa mikrovesikulaarista, mikä viittaa rasvapisaroiden laajenemisen häiriöön. Entsyymin toiminnan estäminen aiheutti myös maksasolujen hypertrofiaa ja maksavauriota. Rasvaisen ruokavalion aiheuttamia morfologisia ja toiminnallisia muutoksia arvioitiin histologisen kuvananalyysin, elektronimikroskopian ja mikroultraäänikuvantamisen avulla. Huomattavaa oli, että LiB12cKO-hiiret olivat vastustuskykyisiä rasvaisen ruokavalion aiheuttamalle liikalihavuudelle ja maksan rasvoittumiselle, mikä osoitettiin sekä kuva-analyysillä että täydentävillä biomarkkereilla. Nämä havainnot vahvistettiin LiB12cKO-uroksilla todetuilla geenien ilmentymismuutoksilla, mikä viittaa siihen, että HSD17B12:n toiminnan estäminen muuttaa maksan morfologiaa ja rasva-aineenvaihduntaa ja voi tarjota uuden lähestymistavan liikalihavuuden ehkäisyyn.

AVAINSANAT: Kuva-analyysi, hiirimalli, HSD17B12, metabolinen rasvamaksatauti, MASLD

Table of Contents

Abbreviations

AI	Artificial intelligence
ALT	Alanine aminotransferase
AST	Aspartate aminotransferase
BD	Bile duct
CDAHFD	Choline-deficient, L-amino acid-defined high-fat diet
CE	Cholesteryl ester
CER	Ceramide
CNN	Convolutional neural network
CRN	Clinical Research Network
CT	Computed tomography
CV	Central vein
DL	Deep learning
ER	Endoplasmic reticulum
FC	Fold change
GGT	Gamma-glutamyl transferase
GPX2	Glutathione peroxidase 2
GM	Genetically modified
HCC	Hepatocellular carcinoma
HCD	High cholesterol diet
HDL	High-density lipoprotein
HE	Hematoxylin and eosin
HFD	High-fat diet
HFFD	High-fat high-fructose diet
HSC	Hepatic stellate cell
HSD17B	Hydroxysteroid 17-beta dehydrogenase
IHC	Immunohistochemistry
IR	Insulin resistance
KO	Knockout
LD	Lipid droplet
MASL	Metabolic dysfunction-associated steatotic liver disease
MASH	Metabolic dysfunction-associated steatohepatitis

MAFLD	Metabolic dysfunction-associated fatty liver disease
MCD	Methionine-choline deficient diet
ML	Machine learning
MRI	Magnetic resonance imaging
NAFLD	Non-alcoholic fatty liver disease
NASH	Non-alcoholic steatohepatitis
ORO	Oil Red O
PAS	Periodic Acid Schiff
PPAR	Peroxisome proliferator-activated receptor
PSR	Picro sirius-staining
PT	Portal tract
QUS	Quantitative ultrasound
RGB	Red-green-blue
ROI	Region of interest
SM	Sphingomyelin
STZ	Streptozotocin
TEM	Transmission Electron Microscopy
TUNEL	Terminal deoxynucleotidyl transferase dUTP Nick End Labeling
UBM	Biomicroscopy
VFM	Vision Foundation Model
WSI	Whole slide image
WT	Wildtype
XAI	Explainable artificial intelligence
2D	Two-dimensional
3D	Three-dimensional
µUS	Micro-ultrasound

List of Original Publications

This dissertation is based on the following original publications, which are referred to in the text by their Roman numerals:

I **Mairinoja L**, Heikelä H, Blom S, Kumar D, Knuuttila A, Birkman E-M, Ruusuvuori P, Strauss L, Poutanen M. Deep-learning based image analysis of liver steatosis in mouse models. *The American Journal of Pathology*, 2023; 193(8), pp. 1072-1080.

II Heikelä H, **Mairinoja L**, Ruohonen S, Rytkönen K, de Brot S, Laiho A, Koskinen S, Suomi T, Elo L, Strauss L, Poutanen M. Disruption of HSD17B12 in mouse hepatocytes leads to reduced body weight and defect in the lipid droplet expansion associated with microvesicular steatosis. *FASEB*, 2024; 38(17), e70034.

III **Mairinoja L**, Heikelä H, Ekwe D, Ojo O, Kukoricza K, de Brot S, Eskelinen E-L, Strauss L, Poutanen M. HSD17B12 inactivation is a novel approach for reducing weight gain and development of liver steatosis resulting from a high-fat diet. *Manuscript.*

1 Introduction

Metabolic dysfunction-associated steatotic liver disease (MASLD), and its more severe form metabolic dysfunction associated steatohepatitis (MASH), are the hepatic manifestation of metabolic syndrome and their incidences are continuously growing worldwide, along with obesity (Pipitone et al., 2023; Younossi & Henry, 2024). Mouse liver is similar to the human liver both structurally and functionally, and therefore mice represent valuable models for investigating human hepatobiliary physiology and disease pathogenesis (Rogers & Dintzis, 2012). The hallmarks of MASLD are micro- and macrovesicular lipid droplets (LDs) accumulating inside the hepatocytes (Chalasani et al., 2018), whereas when MASLD develops to MASH, fibrosis and inflammation are present. MASH may lead to cirrhosis, in which the liver is scarred and permanently damaged. There are several mouse models mimicking these different aspects of MASLD and MASH, including genetically modified (GM) mice, mice treated with obesogenic diet and with nutritional insult (Fang et al., 2022; Flessa et al., 2022). In order to fully understand the disease mechanisms in detail, novel methods to study efficiently the MASLD and MASH manifestations, and effects of drug treatments in preclinical models *in vivo* and *ex vivo* are needed.

Biomedical imaging is a key concept in clinical and preclinical research. The advancement of imaging modalities and image acquisition techniques in biomedical applications has significantly contributed to the exponential growth in image data volume. This surge in data has, in turn, created a heightened demand for effective image analysis. While the fundamental principles for extracting meaningful information from images have been well-established for decades, there remains ongoing work in optimizing and applying various analytical methods to address specific biological questions. Despite significant progress in the field, challenges persist in developing tailored solutions that enhance the accuracy, efficiency, and relevance of image analysis in diverse biological contexts. In this study, new image analysis methods and workflows were developed for histopathology and *in vivo* -imaging to detect MASLD-related changes in mouse liver accurately, effectively and reliably.

We have previously shown that disruption of the function of the hydroxysteroid (17β) dehydrogenase enzyme (HSD17B12), known to be involved in the lipid metabolism, leads to liver steatosis (Heikelä et al., 2020). However, the specific role of the HSD17B12 in the liver lipid metabolism is still unknown. In this work, the role of HSD17B12 enzyme in the development of MASLD was studied by using hepatocyte-specific HSD17B12 knockout mouse model (LiB12cKO). We showed with image analysis, that LiB12cKO mice on a chow diet exhibited significant liver fat accumulation with reduced overall body fat, primarily in the form of microvesicular steatosis, indicating impaired lipid droplet expansion. Despite this, LiB12cKO mice were resistant to high-fat-diet-induced obesity and liver steatosis.

In the process of writing this thesis, selected artificial intelligence (AI) tools were employed to aid in various stages of the research. Keenious, Elicit and Scite were utilized for literature search. DeepL, Copilot and ChatGPT were employed to assist with refinement of the English language. After using these tools, the author reviewed and edited the content and take full responsibility for the content of the thesis. AI-based tools were applied in the image analysis, and a comprehensive description of these tools and methods are presented in the methods section.

2 Review of the Literature

2.1 Imaging and image analysis of the mouse liver

Mouse models are needed in preclinical research because they enable the study of biological processes, diseases, and potential treatments in a living system. Mouse liver shares many physiological similarities with human liver, and therefore, it is suitable for translational research. The assessment of liver diseases has become a critical focus in medical and biomedical research due to the global burden of liver-related conditions (Younossi, Wong, et al., 2023). Developing accurate and reliable methods is essential for monitoring disease progression and evaluating therapeutic interventions in preclinical models. Histopathology is the traditional method to assess liver diseases, combined with serum liver biomarkers (such ALT, AST and GGT) with elevated levels indicating hepatocellular injury (Parsons, 2023). In addition to histopathology, a range of *in vivo* imaging techniques have been introduced. Liver ultrasound is common clinical *in vivo* method, while magnetic resonance imaging (MRI)- and computed tomography (CT) -based methods are also utilized to improve diagnostic precision and reduce the invasiveness of assessments (Dana et al., 2022). The same modalities employed in clinical settings have also been adopted in preclinical research. However, the primary focus in the latter is on generating reproducible and quantitatively comparable data.

2.1.1 Digital and computational histopathology

Histology is a field that focuses on the analysis of the structure, development and function of cells and tissues on a representative section using microscopy as its main tool (Betyna & Zieliński, 2018). Tissue sections have been examined under the microscope as early as the 19th century, and the method remains central to many fields, including biology, biomedicine and medicine, especially pathology. Today, in addition to and instead of microscopic examination, samples are often digitised, allowing the examination of samples on a computer screen instead of a microscope (Aeffner et al., 2018).

Histopathological assessment aims to identify cellular abnormalities and determine the presence and extent of structural changes. Human visual system is

well suited for interpreting and combining visual information and some tasks are easy for human visual system, such as understanding concept based on surroundings, and rapid pattern detection (Kaiser et al., 2020). These are also key concepts in histopathological assessment. However, some tasks are very difficult to human eye, those including continuous monotonic tasks and quantification of only slightly different intensities. Computer aided quantitative analysis can ensure repeatability and reproducibility, reduce subjectivity and variation between observers. In order to increase efficiency, the field of pathology is currently taking a significant step toward by digitalization of the entire workflow, from staining to analysis, due to great advances in computational power and whole slide scanner technology (Aeffner et al., 2018). Computational analysis and machine learning can provide enhanced diagnostic accuracy, facilitate the identification of patterns in tissue samples, and enable the automation of image analysis, ultimately improving workflow efficiency and supporting personalized medicine approaches (Kotian, 2024).

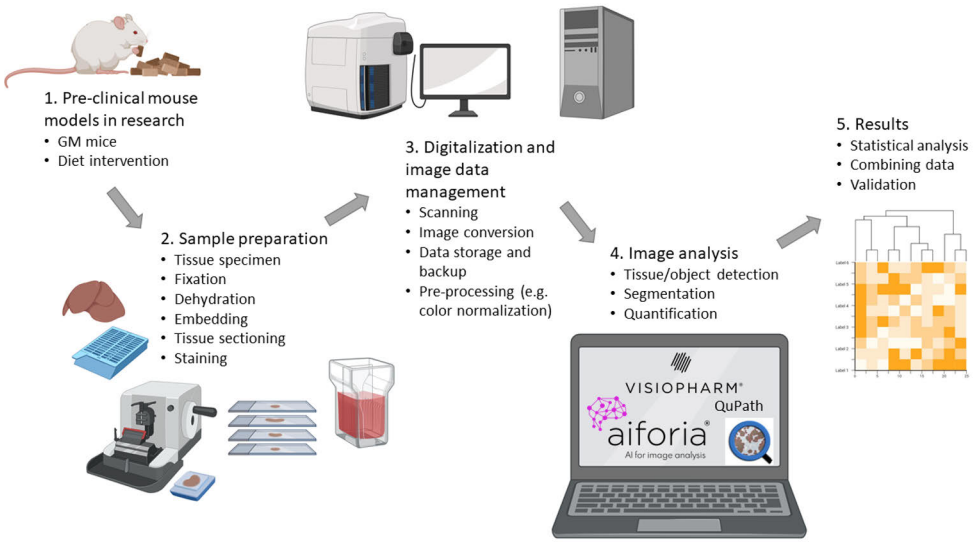

Figure 1. The process of digital and computational histopathology in preclinical research. (1) The process of acquiring relevant, meaningful and correct data starts with experiment design including suitable mouse models and the extent of the experiment. (2) Sample preparation plays a crucial role in what type of data can be obtained from the images. (3) Image analysis pipeline optimization starts with the data acquisition (3). Image analysis process (4) includes usually many steps. The results (5) need interpretation with statistics and graphical representation as well as setting the results in context. Created with BioRender.com.

2.1.1.1 Sample preparation

Histopathology is a science completely dependent upon microscopic examination and interpretation. Correct biopsy procedure, proper fixation and sample processing techniques are essential in order to achieve a conclusive analysis or diagnosis. The complex sample preparation and variation in staining and scanning conditions affect crucially to the image data. The histological image data to be compared should be produced and processed simultaneously to ensure the integrity of data. Understanding of the sample preparation is crucial, since quality control and troubleshooting are essential steps in the image analysis process, and artefacts should not be interpreted as meaningful data in images (Brixtel et al., 2022).

Biopsy procedure includes extracting the organ, or piece of it from living or dead animal or human. It is crucial to understand the orientation of certain organ and how it is placed on mounting cassette, since the final image will visualize only one thin slice of the structure and the whole three-dimensional organ needs to be interpreted from two-dimensional image.

Fixation preserves tissue structures and prevents autolysis and bacterial decomposition. It can be chemical, using agents like formaldehyde or alcohol, or physical, such as heat or cryopreservation (Bancroft & Layton, 2019). Factors like fixation time, temperature, pH, and specimen size influence its success (Qidwai et al., 2014). Improper fixation leads to poor morphology and staining in histological images. In the paraffin block preparation, dehydration removes water and fixative using ethanol, followed by clearing with an agent, such as xylene, which is soluble both with ethanol and paraffin. Tissue sections are then impregnated with paraffin wax for thin sectioning (Feldman & Wolfe, 2014). Wax-embedded blocks are cut into ~5 μm sections with microtome and mounted on glass slides. Paraffin is removed before staining.

Histology images often contain artifacts due to sample preparation issues like staining inconsistencies, tissue folding, or sectioning errors (Taqi et al., 2018). These artifacts can mislead image analysis, excpecially AI models, and reduce diagnostic reliability. There has been effort to overcome these problems, by a pre-processing framework that automatically detects and restores artifacts in histology images (Ke et al., 2023). The framework combines image processing techniques with deep learning models to identify and correct various types of artifacts, and it is designed to be generalizable across different tissue types and staining protocols (Ke et al., 2023). Another example is artifact removal method by Dahan et al. where the weakly-supervised approach reduces the need for fully annotated datasets (Dahan et al., 2022).

2.1.1.2 Staining

The tissue sections are typically stained before they are visualized under microscope. Choosing the right staining is critical. Hematoxylin and eosin (HE) staining is a widely used basic staining and suitable for analysis of general tissue architecture. HE staining was first used by chemist N. Wissozky 1876 and it is still the most common staining because it is simple to use and demonstrates different tissue structures clearly (Bancroft & Layton, 2019). Alkaline hematoxylin stains the cell nuclei dark blue, showing clear intranuclear detail, and acid eosin stains cell cytoplasm and most connective tissue fibres in varying shades and intensities of pink (Bancroft & Layton, 2019). Currently, the routine staining is automated in many laboratories, with automated staining machines and commercially prepared hematoxylin and eosin solutions (Bancroft & Layton, 2019). Specific stainings, such as van Gieson to analyse collagen, or immunohistochemistry can be utilized to study specific structures and molecules.

Immunohistochemistry (IHC) enables visualizing specific biomolecules (antigens), within tissues using antibodies that specifically bind to those antigens. The steps in performing IHC include fixation, paraffin embedding and sectioning, antigen retrieval, selection and preparation of antibody and reagents, incubation, washing, and counterstaining (Kim et al., 2016). The antibodies bind to the targeted epitopes and the targeted molecule can be visualized by using enzyme or fluorescent dye that is linked to the antibody (Taylor, 2014). The technique's effectiveness depends on proper performance, control, and interpretation (Taylor, 2014). IHC method reveals the presence or absence of particular antigens, providing essential information to biomedical research and diagnostic processes.

Recently, virtual staining procedures have been developed to provide more sustainable, rapid, and cost-effective alternatives to traditional histological pipelines (Latonen et al., 2024). E.g. label-free imaging combined with deep learning-based virtual staining has been developed to replicate traditional HE stained slides (Koivukoski et al., 2023). The authors used unprocessed and deparaffinized sections of tissue to capture high-resolution images without applying dyes. Deep learning model is trained to convert these label-free images into realistic virtual HE images that mimic the appearance of chemically stained slides. The method is scalable to whole slide images, making it suitable for clinical and research applications and the goal is to streamline pathology workflows by eliminating the need for chemical staining, which is time-consuming and can degrade tissue samples. Further, the study by Khan et al. showed how different deep learning architectures (e.g., U-Net, CycleGAN, pix2pix) influence the quality and diagnostic utility of virtual HE staining (Khan et al., 2023). In addition, since in certain clinical settings there is a need for faster histologic evaluation, possibility of virtual staining of nonfixed tissue histology have been investigated (Pillar et al., 2024). However, the development of

these technical innovations is in an early phase and requires comprehensive validation, before they are applied more widely.

2.1.1.3 Whole slide imaging

Whole slide scanning involves the digitalization of glass slides to create whole slide images (WSIs). WSI scanner automatically digitizes the entire slide by acquiring microscopic images at one or more resolution and then “stitches” these sequential images into a large composite image (Pantanowitz & Parwani, 2017). Scanners are well-suited for imaging visible stains, such as hematoxylin and eosin (HE) or immunohistochemistry, while fluorescence scanners are specifically used to digitize slides labelled with fluorescent dyes. Viewing software mimic the conventional microscope review (Pantanowitz & Parwani, 2017).

Digital images are composed of small picture elements, called pixels, arranged in array. Pixel values vary by image type. For example, 8-bit grayscale images use values from 0 to 255 (2^8), while 16-bit images use 0 to 65535 (2^{16}). Histological images are notable for their color, typically represented using 24-bit color, which allocates 8 bits each to red, green, and blue channels. This allows for 256 intensity levels per channel, resulting in over 16 million possible color combinations. (Pantanowitz & Parwani, 2017).

As mentioned above, one essential feature of histological images is colors. In many other microscopy methods, such as fluorescence microscopy, the image data is grayscale and colors are created for visualization with different look-up tables. Color normalization in histology involves computational methods to reduce variability caused by differences in staining, scanning, and displays. Key approaches include using color calibration slides with known spectral properties, applying color correction in linear RGB space for efficiency, and generating transformation matrices to align scanned colors with reference standards (Inoue & Yagi, 2020).

Color and illumination normalization is data processing step that is often appropriate, but the selection of an appropriate reference image for the stain normalization is a critical challenge in histopathology image analysis. Many approaches have been developed recently to overcome these challenges. Some studies propose automated, statistically driven methods for selecting reference images that better represent the color distribution of histology datasets, for example for breast cancer (Abdul Jawad & Khursheed, 2024). Another study proposes a unified framework (called RandStainNA) that combines stain normalization and stain augmentation to train models that are robust to stain variations to overcome the challenge of stain variability in histopathology images, which can hinder the generalization of deep learning models across datasets from different labs or scanners (Shen et al., 2022).

Color normalization in histology has become a major research focus due to the increasing reliance on digital pathology and AI-driven image analysis. For example, Khan et al. (2025) presents a comprehensive evaluation of stain normalization techniques in histopathology using a uniquely diverse dataset. They assembled a unique multi-center dataset by distributing colon, kidney, and skin tissue blocks to 66 labs for routine HE staining, controlling all other variables. Using this dataset, eight stain normalization methods was benchmarked, four traditional (histogram matching, Macenko, Vahadane, Reinhard) and four deep learning-based (CycleGAN and Pix2pix, each with two variants), through both quantitative and qualitative evaluations (Khan et al., 2025).

In general, the appropriate resolution depends on what is being observed. The resolution must be high enough so that objects relevant to diagnostics or other analysis, such as cells, intracellular organelles, or other tissue components, can be clearly distinguished. A higher resolution means a larger data size, which makes analyses more difficult because more computer power is needed. The objective (usually 20x or 40x) and the camera of the whole slide scanner defines the resolution of the WSI, which is often expressed in micrometers per pixel (µm/pixel). In histopathology, 40x is typically used magnification, but it produces an image that is several gigabytes large. However, WSIs created by scanning a histological sample usually contains many resolution levels, and this type of image is called an image pyramid (Figure 2). Pyramidal format stores multiple resolution levels in a single container. By using a tile based pyramidal image format and storing precomputed downscaled versions of the high-resolution images, access can be optimized. In recent years, novel computational methods are being developed to enhance resolution beyond hardware constraints. For example, unsupervised deep learning has been used for enhancing the resolution of hyperspectral histology images (L. Ma et al., 2022).

There is also an effort to modernize the whole process from staining to imaging and even to analysis, by combining label-free imaging with automated whole slide scanning. Tweel et al. developed Photon Absorption Remote Sensing (PARS) Microscopy as a label-free, non-contact, and non-destructive imaging modality for histopathology (Tweel et al., 2023). It proposes an automated WSI system using PARS, enabling further molecular or genetic testing on the same tissue and serving as an alternative to traditional HE staining and brightfield microscopy. Furthermore, a study by McNeil et al. presented a novel, fully automated digital pathology platform that combines hyperspectral autofluorescence (AF) microscopy, deep learning-based virtual staining mimicking HE and Masson's trichrome stains and AI-based MASH scoring based on two-stage deep learning pipeline that segments histological features and predicts MASH CRN (Clinical Research Network) scores (McNeil et al., 2024).

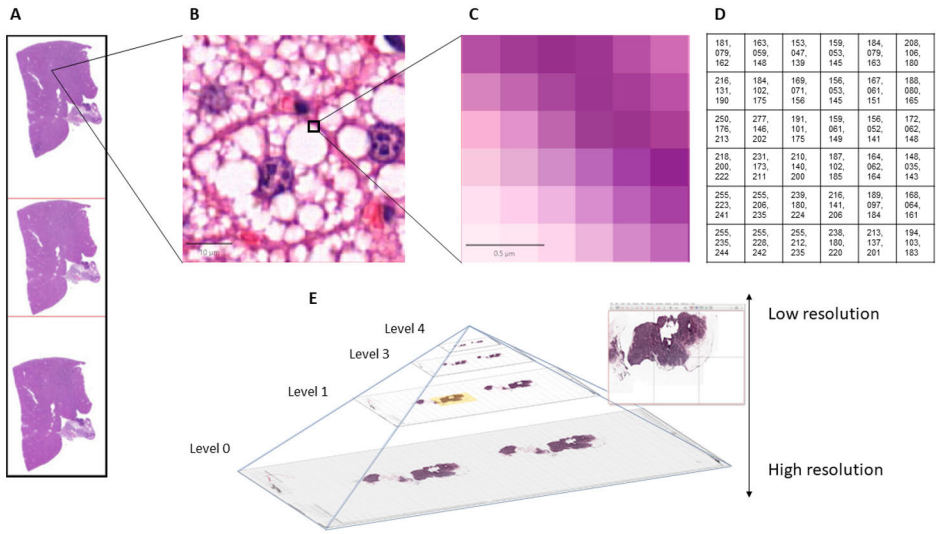

Figure 2. A whole slide image (A) is a collection of pixels, where each pixel has a numerical value (B-D). Image pyramid is a multi-scale representation of an image, allowing observation from low to high resolution (E). One whole slide image can contain 20 billion pixels and 60 GB raw data. E modified from (Bankhead, 2025).

2.1.1.4 Computational image analysis

The histological assessment has been based on visual examination for decades, but recently, standardisation and reproducibility to the whole process of histopathological examination is required (Aeffner et al., 2018). The growing need for quantitative, objective, and accurate analysis tools has driven the development of numerous software packages over the past decade, and as a result, there has been a significant rise in computational methods designed to extract, quantify, and visualize information from microscopy imaging data of biological samples (Haase et al., 2022). Computational image analysis can increase efficiency and ensure repeatability and reproducibility by reducing subjectivity and variation between observers. The first computational image analysis methods were developed in 50s, and AI was invented 70s and 80s, but the computational analysis of images has only fairly recently become an option in histopathology and traditionally the assessment has been based on pathologist's visual evaluation (Irshad et al., 2014). Higher computer power is needed in fields such as histology, which has a high amount of digitized data (Dimitriou et al., 2019). Recently, deep learning (DL) -based methods have become popular in image analysis, because of the development of graphics processing units and more powerful memory resources (Alzubaidi et al., 2021).

Interpreting the three-dimensional (3D) structure of tissues from two-dimensional (2D) sections requires foundational knowledge on physiology and

understanding of histology. In addition to knowing the basic tissue types and to being able to classify them, recognizing pathologic changes is also crucial. Different 3D histology methods have been developed to overcome the limitations of two-dimensional image. For example, tissue clearing methods have been applied enabling fluorescence light sheet microscopy imaging of a tissue piece and then pseudo-coloring was applied to the reconstructed volumes to obtain a final image in the typical HE colors (Laurino et al., 2023). Another approach is to cut a tissue in serial sections and perform computational reconstruction to images. Many algorithms have been developed, tested and compared to assess the accuracy and robustness of different computational approaches in reconstructing biologically meaningful 3D tissue structures (Kartasalo et al., 2018). For example, novel computational techniques are developed for 3D spatial analysis of histological data in cancer biology, focusing on the quantification and visualization of tissue environments at both the organ and tumor levels (Ruusuvuori et al., 2022). Furthermore, Liu et al. introduced a novel method for 3D reconstruction of thick tissue blocks using systematic 2D histological sections, with a specific application in understanding palatal shelf elevation, which is a critical developmental process in mammalian palatogenesis (Liu et al., 2021).

In histopathological images one color might represent a certain biological structure. However, since it is not in its own channel, sometimes useful approach for image analysis is to extract different colors from the image. One approach is to use colour deconvolution (Ruifrok & Johnston, 2001) which is implemented in many commercial and open source bioimaging software applications. The procedure takes an RGB image as input and returns three 8-bit images with color look up tables that correspond to the respective vector colors, i.e. it unmixes the dyes.

IHC is commonly used to both localize and quantitate different biomolecules, such as proteins. While it provides valuable spatial and contextual information, it is generally regarded as semiquantitative rather than fully quantitative. Combinative semiquantitative scoring is commonly used method by pathologists to assess IHC images, and it combines the assessment of relative percentage of immunopositive cells as previously described, and evaluation of the intensity of the staining (S.-W. Kim et al., 2016). The intensity is commonly scored from 0 to 3 (0, negative; 1+, weak positive; 2+, moderate positive; and 3+, strong positive). The final immunoscore is calculated by adding or multiplying each score. Furthermore, IHC is considered to be semiquantitative, because antigen-antibody reactions are not stoichiometric, meaning that the darkness of stain does not equate to the amount of expression of a given antigen (Walker, 2006). In fact, most histological stains are non-stoichiometric. In addition, IHC results can vary significantly due to technical variability and subjective interpretation (Taylor & Levenson, 2006). From an image analysis perspective, quantifying staining intensity is a relatively simple task. However, using this data to

estimate exact concentrations of target expression can be misleading. Instead, image analysis of IHC is best suited for providing spatial info and relative measurements and comparative data (e.g., more or less expression between samples).

2.1.1.5 Machine learning and deep learning based histopathological assessment

Image analysis has historically relied on traditional computer vision methods, which were developed using rule-based algorithms and handcrafted features. These classical techniques have been refined over decades and laid the foundation for modern approaches. Traditional approaches typically follow a similar analytical pipeline that includes image acquisition, segmentation, post-processing, feature extraction, object classification, and validation. Among these steps, image segmentation is particularly critical. It involves isolating objects of interest from the background and serves as a foundational step for subsequent analysis. Accurate segmentation enables the identification of regions of interest (ROIs), from which quantitative measurements can be extracted. In recent years, artificial intelligence (AI), particularly machine learning and deep learning, has transformed image analysis by enabling systems to learn patterns directly from data.

Recent advances have introduced machine learning (ML) methods that learn directly from data, improving the accuracy and efficiency of histopathological workflows (Cooper et al., 2023). In machine learning, relevant features are extracted from the object to be detected in the image and based on that, an algorithm describes or predicts the object. Key benefits of ML include reducing manual workload, minimizing human error and inter-observer variability, and enabling analysis of large datasets efficiently (Cooper et al., 2023).

Deep learning (DL) is a subset of machine learning that enables computational models to autonomously learn features from digitized images for the purpose of image analysis. DL is based on artificial neural networks, which consist of multiple layers of interconnected nodes, each of which performs specific computations (LeCun et al., 2015). The number of neurons and layers can vary. Input data has values that are recalculated with weights. During the training process, the weights are iteratively updated to improve the output. Supervised deep learning is a subfield of deep learning where a model is trained on a labelled dataset using deep neural networks.

In image analysis, convolutional neural networks (CNN) are the most commonly used DL method. In convolutional neural networks, the convolution operation is used at least on one of the layers of the deep neural network (LeCun et al., 2015). Deep learning and CNNs are particularly effective for image classification, segmentation, and detection tasks in histopathology, since histopathological images are rich in structural and phenotypic information (Banerji & Mitra, 2022).

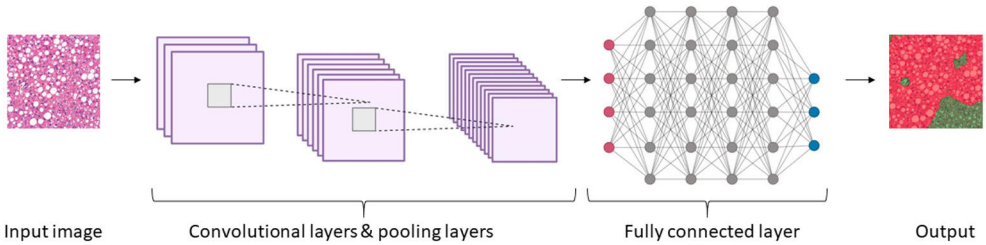

Figure 3. Convolutional neural network (CNN) applied to histology image analysis. The input histological image undergoes feature extraction through convolutional and pooling layers, followed by classification in fully connected layers, producing an output such as tissue segmentation or pathology prediction. Created with BioRender.com.

Transfer learning, data augmentation, and patch-based analysis are common strategies to handle large WSIs (Ahmed et al., 2022). Patch-based analysis involves dividing WSIs into smaller, manageable patches, since their extremely large size makes it computationally infeasible to process them in full. These patches serve as the primary input for deep learning models, enabling efficient processing and analysis without compromising spatial detail. Data augmentation is a technique to artificially increase the size and diversity of the training dataset by applying transformations to the image patches, in order to help prevent overfitting, to improve model robustness, and to simulate real-world variability in tissue appearance and staining (Ahmed et al., 2022). Transfer learning means using a model pre-trained on a large dataset and fine-tuning it on histopathology data, in order to reduce the need for large labelled datasets in histopathology and speed up training while improving performance.

However, there are some challenges that are characteristic when applying DL to histopathology. These challenges include color variability due to staining differences across laboratories, lack of labeled data and annotations, especially at the pixel level, as well as that high resolution of WSIs makes direct processing computationally expensive (Banerji & Mitra, 2022). In addition, differences in instrumentation and image quality (brightness, contrast, resolution/pixel size etc.) introduce domain shifts in histopathology images (Stacke et al., 2021).

In recent years, research in deep learning has increasingly focused on self-supervised learning methods. In the domain of image analysis, Vision Foundation Models (VFMs) have emerged as a promising alternative to traditional supervised CNNs (Chen et al., 2023). In the field of image analysis, Vision Foundation Models (VFMs) are trained based on self-supervised methods on large unlabeled datasets with different qualities and diversities of nature images, producing universal features applicable to various visual tasks (P. Liang et al., 2025). An emerging development in the field of image analysis involves the integration of generative language models with image analysis. For example, PathAlign is a vision-language model tailored for digital pathology and WSIs (F. Ahmed et al., 2024). It addresses the persistent

challenge of aligning whole slide images with pertinent segments of pathology reports, which represents a critical limitation in current multimodal learning frameworks. Allowing researchers to receive analysis results simply by asking questions through AI tools would speed up the workflow and eliminate the need for specialized skills in image analysis or knowledge of its processes. At the same time, it would make the use of AI more non-transparent in everyday research practice.

2.1.1.6 Image analysis of MASLD and MASH in mouse liver

Histological image analysis of MASLD and MASH in mouse liver models is shifting from visual inspection to use of computational methods. Various methods and tools have been developed, especially with the integration of artificial intelligence and advanced imaging techniques, to detect and quantify MASLD and MASH related histologic features.

Common approach to study liver steatosis in mice is to use hematoxylin-eosin (HE) -stained liver tissue sections for generating algorithms to detect lipid droplets (Baek et al., 2023; Guo et al., 2019; Roy et al., 2020). Examples of deep learning based histopathological assessment of mouse liver include a deep learning algorithm that was developed to quantify fatty vacuoles in mouse liver models of MASLD (Ramot et al., 2020). This algorithm uses a segmentation framework to differentiate vacuoles from liver blood vessels and bile ducts, showing a strong correlation with traditional semiquantitative methods ($r = 0.87$, $P < .001$) (Ramot et al., 2020). Deep learning models have been used to detect hepatocellular hypertrophy in rat liver, showing strong correlation with traditional methods and improving the accuracy and repeatability of diagnoses (Pischon et al., 2021).

In addition, AI algorithms have been used to quantify liver fibrosis in preclinical models (Hwang et al., 2023; Ramot et al., 2021). Fibrosis, ballooning inflammation and steatosis has been quantified from Masson's trichrome stained samples with CNN based model (Heinemann et al., 2019). By using the same dataset, an unsupervised transfer learning model for NASH scoring and fibrosis staging was developed years later (Karagoz et al., 2023). Deep learning models to measure fibrosis in PSR stained images has been also developed (H.-J. Kim et al., 2023; Yu et al., 2018).

Furthermore, algorithms to provide spatial information of steatosis have been developed, such as a DL model for zonated quantification of steatosis in an entire mouse liver (Schwen et al., 2016). However, similar to many existing models, this approach does not enable the detection or quantification of microvesicular steatosis.

In the field of liver histopathology, AI models have been reported to achieve high accuracy in tasks such as steatosis quantification, fibrosis staging, and drug-induced liver injury classification (Grignaffini et al., 2024). However, the development of

standardized datasets and benchmarks for liver histopathology, as well as the integration of multimodal data for predictive modeling, are essential to fully realize the potential of these models (Grignaffini et al., 2024).

2.1.2 Transmission electron microscopy

Transmission Electron Microscopy (TEM) is an imaging technique, that employs a beam of electrons instead of light to visualize specimens, allowing researchers to observe cell and tissue structures in nanometer resolution. The acceleration voltage of routine instruments is 100-200kV and since the electrons interact strongly with atoms by elastic and inelastic scattering, the specimen must be very thin, typically 5-100 nm (Reimer & Kohl, 2008). Special sample preparation techniques are needed for this, meaning ultramicrotomy of stained and embedded tissues or cryofixation in biosciences.

The sample will undergo certain number of stresses (mechanical, chemical, ionic, physical) during sample preparation and observing it in TEM as well as some artefacts are always present (Ayache et al., 2010). In addition, what is observed in the TEM is an infinite small representation of the sample (considering the surface area and the volume), therefore, the sample being analysed does not correspond exactly to the original subject we are investigating. However, it allows the study of intracellular structures for which the resolution of light microscopy methods are not sufficient.

Applications of TEM in studying steatotic liver disease include the assessment of organelle integrity and distribution within liver cells. For example, Zhang et al. reported that in steatotic liver tissue in rats, examined via TEM, there was evident fragmentation of the endoplasmic reticulum (ER), alongside the presence of autophagosomes, which are critical indicators of cellular stress and damage related to lipid accumulation (Zhang et al., 2019). Also mitochondrial changes in mouse hepatocytes have been studied with TEM in order to study the effects of a natural therapeutic agent, echinacoside, to MASLD (Yan et al., 2024). In addition, the effects of fasting and obesity on hepatocellular structures and functions, particularly ER, have been investigated in mice combining TEM, Focused Ion Beam Scanning Electron Microscopy (FIB-SEM), deep learning-based segmentation analysis, and high-resolution fluorescence imaging (Parlakgül et al., 2024).

2.1.3 Micro-Ultrasound imaging of mouse liver

Ultrasound refers to sound waves that are not detectable by the human ear, thus frequencies greater than 20,000 cycles/sec (Hz). Diagnostic ultrasound commonly uses frequencies between 2 and 15 MHz (10^6 cycles/sec). Ultrasound has many advantages, such as ease of use, portability, accessibility, relatively low cost and non-invasiveness. However, it is a subjective and observer dependent method.

Micro-ultrasound (μUS), also called ultrasound biomicroscopy (UBM), refers to the use of high-frequency ultrasound (typically >20 MHz) to achieve images of tissues and organs that are too small to be resolved with conventional ultrasound (Lockwood et al., 1996). In mice, common applications of micro-ultrasound are to image heart, other organs and tumors, and to visualize and guide injections into target organs (Cootney, 2001). Since the axial and lateral resolution improves with increasing frequency, higher frequency transducers are preferred for rodent imaging (Cootney, 2001). High-frequency ultrasound systems employing transducers in the 40–60 MHz range can achieve spatial resolutions approaching 50 μm, owing to their narrow beam widths and short wavelengths (Foster et al., 2000). Although such systems typically exhibit limited penetration depths of approximately 1-2 cm, this constraint is not prohibitive for small animal imaging applications, such as rats and mice, where most of the target organs are generally within the penetration depth range (0.5-2 cm) of the higher frequency transducers (Cootney, 2001).

The common imaging formats are brightness mode (B-mode), motion mode (M-mode), spectral Doppler, and color Doppler. B-mode ultrasound is the most widely used imaging modality for assessing hepatic steatosis in clinical settings. This technique enables qualitative grading of liver fat accumulation based on several characteristic findings: 1) increased echogenicity of the liver relative to the renal cortex, 2) reduced visibility of intrahepatic vessels, due to increased sound wave scattering 3) impaired visualization of the diaphragm and posterior right hepatic lobe due to ultrasound beam attenuation (Park et al., 2022).

There has been some effort to utilize quantitative ultrasound methods (QUS) to study liver steatosis in humans (Pirmoazen et al., 2020). Latest technical developments allow ultrasound devises to obtain raw radiofrequency (RF) data in addition to images (Mamou & Oelze, 2013). QUS methods include controlled attenuation parameter (CAP), attenuation (AC) and backscatter coefficients (BSC), computerized calculation of hepatorenal index (HRI) and speckle statistics, that include acoustic structure quantification (ASQ) and Nakagami imaging, Speed of sound (SoS), Shear wave elastography (SWE) and quantitative ultrasound (QUS) spectroscopy (Pirmoazen et al., 2020).

However, in preclinical research, ultrasound is not commonly used to study liver steatosis. Liver echogenicity relative to the kidney is used to qualitatively indicate hepatic steatosis and has been shown to correlate well with histological findings in rats (Lessa et al., 2010). In addition, a contrast-enhanced ultrasound method has been developed to evaluate steatotic liver disease progression in mouse models (Pandit et al., 2019). Only few studies are found, where a standard ultrasound equipment is used to quantitatively follow the accumulation of fat in the liver (Di Lascio et al., 2018; Faita et al., 2018).

2.2 Steatotic liver disease

2.2.1 The structure and function of the liver

The liver has an essential role in metabolism and regulating various physiological processes. Liver metabolizes toxic compounds and drugs via hepatic detoxification (Alamri, 2018). Due to large vascular capacity of the liver and abundance of phagocytes (Kuppfer cells), it works as a filter by removing foreign particulate matter, including bacteria, endotoxins, parasites, and aging red blood cells (Suchy et al., 2017). Furthermore, the liver is involved in the metabolism of hormones and it also participates in the regulation and production of circulating plasma proteins including albumins, lipoproteins, and glycoproteins. Liver produces and stores compounds, such as carbohydrates, lipids, vitamins and nutrients and release substance into the bloodstream (e.g. glucose) (Suchy et al., 2017). Liver regulates blood glucose levels, and produces and secretes bile and cholesterol (Alamri, 2018).

The human liver is organized in hexagonal lobules. Each lobule is composed of central vein at its center and six portal triads at each of the six corners that are composed of branches of the hepatic artery, portal vein and bile duct (Suchy et al., 2017). Each lobule can be divided into three zones. Zone 1 accommodate the periportal hepatocytes and is the most oxygenated zone, while zone 3 (centrilobular) is least oxygenated and zone 2 is between zones 1 and 3 (Suchy et al., 2017). Blood flows from zone 1 to 3 and bile from 3 to 1 (Figure 4).

The liver parenchyma consists of mainly hepatocytes (~80%), which are polygonal shape epithelial cells. The nucleus is relatively large and centrally located and quite often hepatocytes with two nuclei are present. Other cell types in the liver include biliary epithelial cells (cholangiocytes), stellate cells, Kupffer cells, and liver sinusoidal endothelial cells (Trefts et al., 2017).

Due to active metabolism, hepatocytes contain relatively abundantly mitochondria, endoplasmic reticulum (ER) and Golgi apparatus. In addition, hepatocytes can have 200-300 peroxisomes per cell. Peroxisomes are 0,2-1,0 μm in diameter and their primary function is lipid metabolism, since they contribute to the breakdown and detoxification of fatty acids (Pawlina, 2024). Cholesterol is converted into bile acids in the liver through several enzyme-driven pathways. Peroxisomes play an important role in the bile acid biosynthesis, that involves modification of the ring structure of cholesterol, oxidation and shortening of the side chain, and finally conjugation of the bile acid with an amino acid (Ferdinandusse & Houten, 2006). Peroxisomes affect cell hypertrophy through mechanisms involving Peroxisome proliferator-activated receptor (PPAR) activation, oxidative stress, mitochondrial interaction, and lipid metabolism. PPARs are crucial in regulating lipid metabolism and peroxisome proliferation. Activation of PPARs leads to

transcriptional induction of fatty acid metabolizing enzymes, which is associated with hepatocellular hypertrophy (Río, 2013).

Human liver is quite similar to mouse liver from its structure and function (Kruepunga et al., 2019). The lobes in human liver are right, left, caudate and quadrate, of which the right is largest. In turn, the lobes in mouse liver are middle (left medial), left lateral, right lateral, and caudate, of which the left is largest (Rogers & Dintzis, 2012). Median lobe is sometimes referred to a fifth lobe in mouse liver, and sometimes as part of the left or right lobe depending on classification (Kruepunga et al., 2019). Each lobe has its own arterial and portal vascularization and individualized biliary drainage. The structural unit containing the portal vein, hepatic artery, and bile duct is called the portal tract.

Unlike the human liver, which is located in the right upper quadrant of the abdomen, the mouse liver spans the entire subdiaphragmatic space (Rogers & Dintzis, 2012). From the histological perspective, human liver has prominent fibrous septa between lobules, but mice have minimal fibrous separation, contributing to the less distinct lobular appearance.

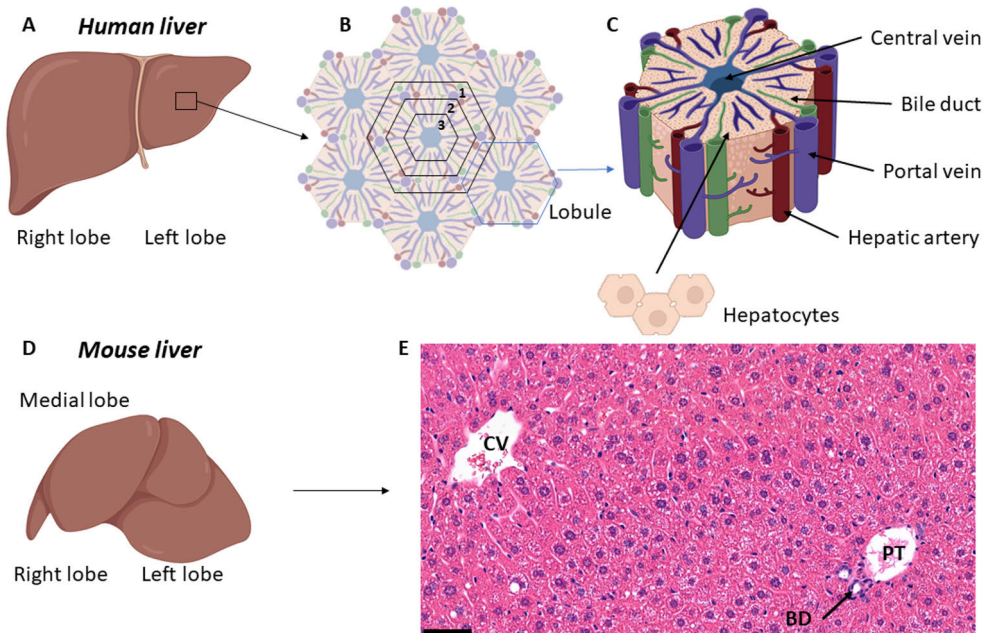

Figure 4. Human liver consists of four lobes, of which two are visible in anterior view (A). The liver is organized in hexagonal lobules that can be divided into three zones: 1. periportal; 2. midzonal; 3. centrilobular (B). Each lobule is composed of central vein at its center and the hepatic artery, portal vein and bile duct in the corners (C). Mouse liver consists of five lobes (D). Mouse liver has similar structure than human liver, but the hexagonal lobules are not apparent (E). HE-stained normal mouse liver tissue, where central vein (CV), portal tract (PT) and bile duct (BD) are visible. Scale bar 50µm. Created with BioRender.com

2.2.2 Metabolic dysfunction-associated steatotic liver disease

Metabolic dysfunction-associated steatotic liver disease (MASLD) is a complex liver disease, but also multisystemic disease associated with metabolic abnormalities (Pipitone et al., 2023; Younossi & Henry, 2024). The disease was formerly known as non-alcoholic fatty liver disease (NAFLD), but because of the epidemiological and pathophysiological link between NAFLD and metabolic disorders, metabolic dysfunction-associated fatty liver disease (MAFLD), and later MASLD, has been proposed as the more appropriate term (Rinella et al., 2023). In addition, the term NAFLD has led to many patients trivializing their condition and further, a word "alcohol" and "fatty" in disease name is a societal burden to NAFLD (Gofton et al., 2023). The liver synthesizes fatty acids from non-lipid sources and assembles lipoproteins for energy transport. Under healthy conditions, it does not serve as a long-term lipid storage, instead packaging excess energy into lipid droplets and lipoproteins for delivery to adipose tissue. Disruption of this balance leads to lipid accumulation in hepatocytes, resulting in hepatic steatosis (Heeren & Scheja, 2021). Steatotic liver disease is characterized by the accumulation of fat in the liver, steatosis, and further MASLD is defined, when at least one of the following metabolic risk factors is present: obesity, high glucose levels or type 2 diabetes, high blood pressure, high plasma triglyserides, or high plasma HDL-cholesterol (Rinella et al., 2023).

The prevalence of MASLD is steadily increasing worldwide as obesity rises, with 30% of the population globally affected (Younossi, Golabi, et al., 2023). Its incidence is three times higher in people with overweight or obesity compared with those of normal weight (Younossi & Henry, 2024). In addition to obesity, it is closely associated with type 2 diabetes and insulin resistance (Targher et al., 2024).

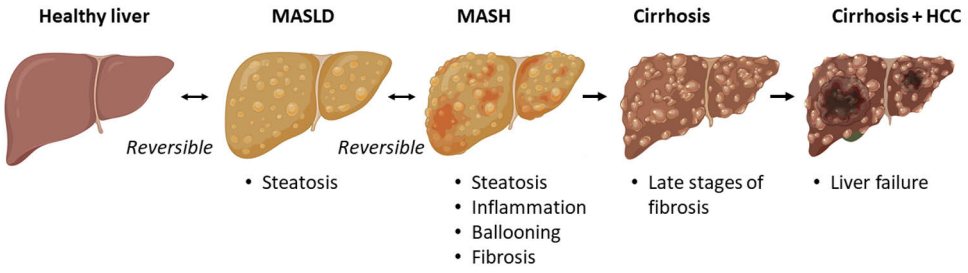

Figure 5. The pathogenesis of MASLD. There is reversibility between healthy liver and MASLD, as well as between MASLD and MASH. Abbreviations: MASLD: Metabolic dysfunction-associated steatotic liver disease; MASH: Metabolic dysfunction-associated steatohepatitis; HCC: Hepatocellular carcinoma. Created with BioRender.com.

2.2.2.1 Metabolic dysfunction-associated steatohepatitis (MASH)

Liver steatosis can still be reversible but if lifestyle changes are not implemented, it eventually develops to metabolic dysfunction-associated steatohepatitis (MASH) or even to irreversible fibrosis, called cirrhosis, and increases the risk for hepatocellular carcinoma (Gadi et al., 2024). MASH was previously known as non-alcoholic steatohepatitis (NASH). MASH is a progressive form of MASLD and is characterized by hepatic steatosis, inflammation, and fibrosis, which can lead to severe liver conditions such as cirrhosis, liver failure, and hepatocellular carcinoma (HCC) (Gadi et al., 2024).

Drugs for steatotic liver disease have long been limited, but recently, GLP-1 receptor agonists have emerged as a promising treatment option (Jensen et al., 2024) These drugs were initially developed for treating type 2 diabetes, but are also widely used for weight management. GLP-1 agonists provide multiple benefits, including weight loss, improved liver enzymes and glycemic control, reduced hepatic fat, and protection against fibrosis by enhancing glucose metabolism, lowering lipogenesis, and promoting fatty acid oxidation (Havranek et al., 2025).

2.2.2.2 Biomarkers of MASLD and MASH

In studies of MASLD and MASH, HE staining is a basic method used to detect fat accumulation and other pathological changes, serving as a histological biomarker of disease progression. Macrovesicular steatosis involves large lipid droplets displacing the nucleus, while microvesicular steatosis features numerous small droplets without nuclear displacement. Other histological features indicating MASH include inflammation, collagen fibers, and ballooning, which is form of hepatocyte injury associated with enlargement, swelling, and characteristic reticulated cytoplasm (Li et al., 2023).

When special stain to highlight the fibrosis is necessary, for example for studying MASH, Masson´s trichrome, van Gieson or Sirius red stains are the most common in use (Clark & Torbenson, 2017). Trichrome stains get the name from the use of three dyes, and they stain smooth muscle red and collagen blue, but do not stain elastic tissue (Clark & Torbenson, 2017). In the Sirius red staining, collagen appears red whereas Van Gieson stains nuclei black, collagen brilliant red, and smooth muscle yellow (Clark & Torbenson, 2017).

Normal hepatocytes contain glycogen, but stronger glycogen deposits can indicate pathology in glycogen storage. In HE-stained paraffin sections, glycogen might show as small holes in the section, similarly to alcohol soluble lipids. Thus, the presence of extra glycogen can be challenging to differentiate from microvesicular steatosis, necessitating the use of specific stains for identifying the correct condition (Farrell et al., 2019). Periodic Acid Schiff (PAS) stains the

glycogen content of hepatocytes red in paraffin sections and Oil Red O (ORO) stains lipids to red-orange color in frozen tissue samples. Therefore, ORO is a well suited method for detecting steatosis in the liver, and for example, the size of the lipid droplets can be quantitated with image analysis methods from ORO stained slides (Ge et al., 2010; Levene et al., 2012).

The TUNEL assay (Terminal deoxynucleotidyl transferase dUTP Nick End Labeling) is a well-established method for detecting DNA fragmentation, a hallmark of apoptosis. This assay labels the 3'-OH ends of fragmented DNA, allowing visualization via fluorescence or colorimetric methods. It is particularly useful in identifying hepatocyte apoptosis, which is indicating liver damage in MASLD and MASH.

IHC markers play a crucial role in the study of liver steatosis and related pathologies. For example, Ki-67 is commonly used to assess hepatocyte proliferation, providing insight into regenerative activity. Cytokeratin-18 (CK-18) is a well-established biomarker of hepatocyte cell death (Neuman et al., 2014). CD68 is widely used to evaluate Kupffer cell aggregation and distribution, particularly in MASH, while Clec4F (C-type lectin domain family 4 member F) is highly specific for Kupffer cells in murine models (Lefkowitch et al., 2002). To assess hepatic stellate cell (HSC) status, desmin serves as a marker for quiescent HSCs, whereas α-SMA (alpha-smooth muscle actin) indicates their activation, which is a hallmark of fibrogenesis. Keratin 8/18 staining enhances the detection of hepatocyte injury and ballooning degeneration, key features of steatohepatitis (Guy et al., 2012). In addition, IHC markers can provide important spatial information, and image analysis methods have been established for example to quantify the zonated location of IHC stains within the liver lobule in normal and steatotic livers (Peleman et al., 2023).

Traditional serum biomarkers include alanine aminotransferase (ALT) and aspartate aminotransferase (ALP) to assess hepatocellular injury; alkaline phosphatase (ASP), which is elevated in cholestasis or bile duct obstruction; gamma-glutamyl transferase (GGT), an enzyme involved in glutathione metabolism and often elevated in biliary tract diseases and alcohol-related liver injury, and bilirubin that indicates liver's ability to process hemoglobin and albumin, which is marker of liver synthetic function (Parsons, 2023). Total cholesterol, triglycerides, and C-peptide reflect metabolic dysfunction and insulin resistance (Neuman et al., 2014). Emerging biomarkers include adiponectin which is typically decreased in MASLD and thus inversely correlated with steatosis severity, whereas leptin, which is associated with inflammation and fibrosis, is often elevated in MASLD (Neuman et al., 2014). Tumor necrosis factor-alpha (TNF-α) is a pro-inflammatory cytokine implicated in hepatocellular injury and fibrosis (Neuman et al., 2014).

2.2.3 Mouse models of steatotic liver disease

Mice are widely used models to study human disease and develop novel pharmacotherapies due to its small size, low-cost and ease in genetic engineering (Fang et al., 2022). Different mouse models are used to simulate various stages of steatotic liver disease induced by dietary and genetic intervention, due to the physiological similarities between mice and humans. An ideal animal model would reproduce the complex pathomechanism of human disease pathology with high resilience (Fang et al., 2022). However, there are also limitations of mouse models in studying human metabolic diseases. Mice and humans differ in metabolic rate, immune responses and gene regulation. In addition, environmental and microbiome factors are highly controlled in laboratory mice, unlike the variability in human populations (Farooqi & Xu, 2024).

2.2.3.1 Dietary models

Diet-induced mouse models are commonly used in the research of steatotic liver disease since they mimic diet-induced obesity and insulin resistance (IR), which are common risk factors for steatotic liver disease in humans.

High-fat diets (HFD) are commonly used and they vary in nutrient composition and amounts of fat. The range in fat content is usually between 45% and 75% of the total calorie intake, and the most typical diet consist of 60% fat, 20% protein and 20% carbohydrates (Flessa et al., 2022). Mice fed with HFD will develop obesity, insulin resistance and hepatic inflammation after 16 weeks of feeding, and increased ALT and AST levels after 34 weeks (Fang et al., 2022). However, different strains and genders show different sensitivities to HFD. The HFD model displays similar features to human MASLD/MASH development, but the fibrogenesis process of MASH is less severe in mice than in humans (Hansen et al., 2017).

High-fat high-fructose diet (HFFD) is obtained by adding 10% of fructose to HFD (Fang et al., 2022). Excessive fat and fructose intake cause IR, inflammation and ER stress, and thus HFFD model is useful when studying the role of ER stress and lipid steatosis in MASLD (Fang et al., 2022). The American lifestyle-induced obesity syndrome (ALIOS) diet is designed to mimic aspects of the Western fast-food diet. Mice are fed high-fat chow (45%), including trans fats, with high-fructose corn syrup added to the drinking water, causing obesity, insulin resistance, and liver steatosis, inflammation, and fibrosis in mice (Harris et al., 2020).

The High Cholesterol Diet (HCD) induces hepatic steatosis characterized by minimal inflammation and an absence of fibrosis. It also leads to elevated serum insulin levels, making it a useful model for mimicking early-stage steatohepatitis and metabolic dysfunction (Flessa et al., 2022). The methionine-choline deficient (MCD) diet is a well-established model for inducing MASH in mice. Mice fed with MCD

diet develop significant hepatic steatosis, inflammation, and fibrosis, mimicking human MASH pathology (Gautam et al., 2024). The Choline-Deficient, L-Amino Acid-Defined, High-Fat Diet (CDAHFD) is another model used to induce MASH in mice. This diet results in rapid onset and progression of steatohepatitis, with significant lipid deposition, liver injury, inflammation, and fibrosis. The CDAHFD model is advantageous for its ability to closely mimic human NASH, including changes in hepatic lipidome and bile acid profiles (Fang et al., 2022).

2.2.3.2 Genetic models

Obesity is a significant risk factor for MASLD and the most prevalent genetic models of obesity are leptin (ob/ob) and leptin receptor (db/db) deficient mice. These originally spontaneous mutations are bred into inbred mouse lines for research purposes. Leptin is a peptide hormone that, among other functions, regulate appetite, neuroendocrine function, and energy homeostasis (Dornbush & Aeddula, 2025).

There are numerous genetically modified mouse models used to study the pathogenesis of metabolic liver diseases. Some of these models involve the modification of genes central to lipid metabolism, such as the PNPLA3 and TM6SF2 models, which affect hepatic triglyceride handling and lipoprotein secretion (Fang et al., 2022). Other models target genes involved in inflammatory pathways, including CD36 knockout mice, as well as several well-established models of metabolic-associated steatohepatitis (MASH), such as mice deficient in low-density lipoprotein receptor (LDLR), apolipoprotein E (ApoE), and prostaglandin E2 (Flessa et al., 2022). These models exhibit key pathological features of hepatic inflammation and fibrosis.

One model to study the full spectrum of MASLD, including its progression to MASH, hepatic fibrosis, and hepatocellular carcinoma (HCC) is STZ + HFD mice model (Jeong et al., 2024). In this model, male C57BL/6J mice are treated with low-dose streptozotocin (STZ) and fed a high-fat diet (HFD). STZ is toxic to the insulin-producing beta cells and is used in diabetes models, since high-dose STZ induces type 1 diabetes by destroying beta cells. However, STZ + HFD combination induces the full MASLD spectrum, starting from steatosis to MASH, fibrosis, and ultimately HCC. However, the model is established and validated only with male mice.

Mouse models either lacking or having decreased expression of hydroxysteroid 17B type 13 (HSD17B13) enzyme are used to study MASLD progression (Crane et al., 2024; Luukkonen et al., 2023; Y. Ma et al., 2021; Su et al., 2022; M. Wang et al., 2022). Human GWAS studies suggest that mutations or inactivation of HSD17B13 may lead to resistance to severe forms of MASLD (Abul-Husn et al., 2018; G. Wang et al., 2018). However, HSD17B13KO mice has shown to develop spontaneous hepatic steatosis and increased liver inflammation (Adam et al., 2018;

Y. Ma et al., 2021). Histological analysis showed lipid droplet accumulation, hepatocyte ballooning, and inflammatory cell infiltration. Interestingly, contrasts with earlier mouse studies suggesting that HSD17B13 deficiency might promote steatosis, there are recent studies showing that mice lacking HSD17B13 did not develop spontaneous hepatic steatosis, even under high-fat or Western diet conditions (Crane et al., 2024). Further, mice lacking HSD17B13 mice tend to show reduced fibrosis (Crane et al., 2024; Luukkonen et al., 2023).

The most commonly used experimental setups combine genetically modified mouse models with dietary interventions to better simulate the complex etiology of metabolic diseases.

2.3 HSD17B12

2.3.1 HSD17B enzymes

Hydroxysteroid (17beta) dehydrogenases (HSD17Bs) are enzymes that regulate the synthesis and metabolism of steroids, cholesterol and lipids. HSD17Bs are involved in the interconversion of active and inactive steroid hormones, particularly HSD17B1 converts estrone (E1) to estradiol (E2) and is highly expressed in estrogen producing tissues (Lukacik et al., 2006; Poutanen et al., 1993). This enzymatic activity is significant in various biological processes, including reproductive functions and the regulation of sex steroid metabolism. However, in addition to their role in steroid hormone metabolism, HSD17Bs have been shown to be involved in several other lipid metabolism pathways. For example, HSD17B4 is involved in the peroxisomal β-oxidation of fatty acids (Breitling et al., 2001). HSD17B7 is essential for cholesterol production (Jokela et al., 2010). HSD17B11 is targeted to lipid droplets and the ER, suggesting a role in lipid metabolism (Horiguchi et al., 2008b) and HSD17B13 is an enzyme associated with lipid droplets and is primarily expressed in hepatocytes (Horiguchi et al., 2008a). Inhibition of HSD17B13 have been associated with protection against MASLD progression to MASH (Abul-Husn et al., 2018; Luukkonen et al., 2020, 2023).

2.3.2 HSD17B12

HSD17B12, or 17β-hydroxysteroid dehydrogenase type 12, is an enzyme that plays a critical role in the metabolism of steroid hormones and fatty acids. HSD17B12 is expressed throughout in mammalian tissues, highest expression being found in the tissues linked to energy metabolism, such as liver and adipose tissue (Saloniemi et al., 2012). In subcellular level, the enzymes that elongate palmitic acid and very long chain fatty acids, as HSDs, have been localized to the endoplasmic reticulum (ER)

(Moon & Horton, 2003). Recent studies confirm that HSD17B12 is localized in the endoplasmic reticulum, which is consistent with its role in lipid metabolism and steroid biosynthesis (Sakurai et al., 2006; Tsachaki & Odermatt, 2019). The enzyme is also found in the cytoplasm, indicating its involvement in various cellular processes beyond the ER (Tsachaki & Odermatt, 2019).

In previous studies using genetically modified mice, it has been reported that HSD17B12 is crucial for early embryonic development (Rantakari et al., 2010). Specifically, knockout (KO) blastocysts exhibited reduced proliferation capacity (Rantakari et al., 2010), and mice with a hypomorphic HSD17B12 allele demonstrated impaired prostaglandin synthesis in the ovary, which was linked to defects in meiotic regulation in oocytes (Kemiläinen et al., 2016).

Since the full deletion of HSD17B12 was lethal, inducible models were created. Interestingly, inducing widespread deletion of the *Hsd17b12* gene in adult mouse tissues by crossing the *Hsd17b12* floxed mouse strain with inducible ROSA26-Cre-ERT mice led to a drastic loss of body weight within 6 days postinduction, evidenced by reduced fat and lean mass as well as severe dehydration (Heikelä et al., 2020). In addition to malaise and eventually death within a week, these mice developed microvesicular liver steatosis, highlighting the essential role of HSD17B12 for normal metabolic homeostasis in adult mice (Heikelä et al., 2020).

To find out if the drastic weight loss was due to defects in HSD17B12 in the adipose tissue an adipocyte-specific, tamoxifen-inducible conditional KO mouse strain (aHSD17B12cKO) was created (Heikelä et al., 2020). The model indicated that the loss of HSD17B12 activity in the adipocytes in adult mice is not responsible for the severe metabolic alteration and starvation that was observed in the HSD17B12cKO mice (Heikelä et al., 2020).

3 Aims

The incidence of metabolic dysfunction-associated steatotic liver disease (MASLD) and it's more severe form, metabolic dysfunction-associated steatohepatitis (MASH) are continuously growing worldwide, along with obesity. Therefore, novel methods to study efficiently the MASLD manifestation, and effects of drug treatments in preclinical models are needed. In this work, novel preclinical image analysis workflows for quantifying MASLD and MASH related histological features on tissue sections *ex vivo* were developed, and novel *in vivo* imaging methods to quantify steatosis were applied. With the developed methods we aimed to determine the role of HSD17B12 in the development of steatotic liver disease and explore its potential as target for drug development.

The specific aims of this thesis were:

To develop novel deep-learning based image analysis for quantifying liver steatosis on histological images of preclinical mouse models of MASLD.

To establish and apply novel histological image analysis workflows and *in vivo* -methods to understand the role of HSD17B12 in the mouse liver.

To understand the development of MASLD in the hepatocyte-specific HSD17B12KO mice after an obesity insult with a wide range of imaging modalities, including micro-ultrasound, electron microscopy and deep-learning based and conventional histological image analysis.

4 Materials and Methods

4.1 Animals (II, III)

All animal work was conducted at the Central Animal Laboratory at the University of Turku, Finland, under the animal license numbers 10605/04.10.07/2016, ESAVI41729/2019 and ESAVI/23322/2023, granted by the Animal Experiment Board in Finland. Animal handling was carried out in accordance with the institutional animal care policies that fully meet the requirements as defined in the National Institutes of Health (Bethesda, MD, USA) guidelines on animal experimentation.

Animals were housed at the Central Animal Laboratory at the University of Turku, Turku, Finland, in individually ventilated cages (IVC, Techniplast, Buguggiate, Italy) with approximately 70 air changes per hour. Constant temperature (21 ± 3°C) and humidity (55 ± 15 %) were maintained together with consistent 12h light-dark cycle, with a light change at 7 am and 7 pm. Autoclaved aspen chips were used as bedding (Tapvei Ltd, Harjumaa, Estonia). Soy-free pellets (RM3, Special Diets Services, Essex, UK) and water were available ad libitum. The animals were individually identified by ear markings and housed with littermates, 1-6 mice per cage. Animals were sacrificed with CO2 asphyxiation and cervical dislocation at the ages of 2, 6, or 8 months.

4.1.1 Generation of conditional knockout mice (II, III)

The liver-specific knockout mouse strain LiB12cKO was created by crossbreeding the Hsd17b12 floxed mice (Heikelä et al., 2020) with mice expressing Cre-recombinase under albumin promoter (Postic et al., 1999). The albumin-promoter directs the Cre recombination in hepatocytes, from the time when hepatocytes begin to replace hematopoietic cells in the fetal liver on embryonic day 10 (Murakami et al., 1987; Weisend et al., 2009) and continues until the postnatal age of six weeks (Postic & Magnuson, 2000). This mouse model was published 2024 (Heikelä et al., 2024).

The genetically modified mouse models were, thus, readily available for developing novel methods to accurately quantify the stage of steatotic liver disease

severity and further help us understanding the action of the protein in the liver. In this study, control mice are referred to as wild-type (WT), as their genetic modification is transcriptionally silent.

4.1.2 The diet intervention (III)

Manila software (Laajala et al., 2016) was used to randomly divide the mice into 2 groups of 10 mice each for the diet intervention. Control group mice were fed normal chow (Teklad rodent diet, Inotiv, Wisconsin, USA) and study group mice were fed high fat diet (HFD), (D17010103, Research Diets, Inc. New Brunswick, USA). The chow pellet, HFD pellet and autoclaved tap water from the public supply (Turun vesilaitos, Turku, Finland) were provided for the animals *ad libitum*. The diet intervention lasted for 12 weeks and during this period, the weights of the animals were measured weekly, ultrasound and echoMRI studies were carried out monthly and blood samples were taken fortnightly. At the end of the experiment, the mice were euthanized by CO_2 asphyxiation and cervical dislocation. The liver, kidneys, gonadal fat pads, heart and spleen were taken from all the animals and weighed on the scale AG204 (Mettler Toledo, Greifensee, Switzerland) and thereafter, stored in liquid nitrogen and formalin. Liver samples were also collected for electron microscopy.

4.2 Metabolic studies, serum analysis, triglyseride measurement and RNAseq (II & III)

The body weight of the mice was measured and recorded once every week using a weighing scale PG2002 (Mettler Toledo, Greifensee, Switzerland). The body composition was measured once every month using the EchoMRI-700TM device (Echo Medical Systems, Houston, USA). Food consumption was monitored during study week 6 and 10 by weighting the food pellets in the morning.

Blood sample for determination of serum ALT and AST levels were collected from the lateral saphenous vein of each of the mice without anaesthesia into serum separation tube (BD Microtainer, Becton Dickinson, Franklin Lakes, USA) using glass capillary. After 30minutes, the samples were centrifuged at 10,000 rpm for 2 minutes to separate the serum and stored in -80°C freezer. Serum ALT level was measured from these samples using commercial ALT activity assay kit (Sigma-Aldrich, St. Louis, USA).

To measure liver triglyceride content, about 100 mg was cut from frozen liver sample, weighted and homogenized in 500 µl of ice-cold 0.1% Trixton X-100 in Phosphate buffered saline (PBS) with Tissue Lyser (Qiagen, Hilden, Germany) using 5-mm stainless beads at 100 Hz for 1.5 minutes. The sample was then centrifuged

for 2 minutes at 12,000 relative centrifugal force (RCF) to remove any debris or particulate matter. The supernatant was collected and diluted 1:4 in 0.1% Triton X-100 in PBS before measurement. Serum Triglyceride Determination Kit (Sigma-Aldrich, Missouri, USA) was used to measure the triglyceride concentration according to the manufacturer's instructions but scaled down for 96-well plate. The absorbance was measured at a wavelength of 540 nm with an Ensight multimode plate reader (Perkin-Elmer, Massachusetts, USA).

4.3 Histology (I, II and III)

Tissue samples were fixed in 10% formalin for 24-48 hours and dehydrated in 70% ethanol. Fixed tissues were embedded in paraffin. Four µm thick sections were cut from the left lateral liver lobe or median lobe, and stained with hematoxylin-eosin (HE), with Picro Sirius Red (PSR), and periodic acid–Schiff (PAS) staining following standard procedures.

Ki-67 (Ki-67 Monoclonal Antibody, SolA15, eBioscience™, Thermo Fisher Scientific, Waltham, MA, USA) immunohistochemical staining was performed on tissue sections (4 µm thick) using Labvision™ autostainer (Thermo Fisher Scientific) or manual protocol. Antigen retrieval was performed in citrate buffer (pH 6) (Genemed Biotechnologies, Torrance, CA, USA) using pressure cooker for 20 minutes and sections were washed by 0.05 M Tris-HCl (Reagena, Toivala, Finland) with 0.05% Tween 20 added. The antibody was diluted 1:2000 and incubated at room temperature (RT) for 60 minutes. The sections were incubated with the secondary antibody, rat on mouse HRP-polymer (Biocare Medical, Pacheco, CA, USA), at RT for 30 minutes and counter stained with Mayer's hematoxylin (Histolab Products AB, Västra Frölunda, Sweden) before mounting with Pertex mounting medium (Histolab Products AB).

TUNEL staining was performed on 4 µm thick tissue sections. Antigen retrieval was performed in citrate buffer in microwave followed by blocking the endogenous peroxidase activity by 3% H_2O_2. TUNEL reaction mixture containing TdT and biotin-16-dUTP (Roche Diagnostics GmbH) was applied on the sections and incubated at 37°C for one hour. After that, the reaction was stopped by adding 300 mM NaCl. The sections were blocked with 3% BSA and incubated in ExtrAvidine (Sigma-Aldrich, diluted 1:500 in 1% BSA) for 30 min at 37°C, followed by staining with 3,3' diaminobenzidine (Dako Liquid DAB+ Substrate Choromogen System; Dako North America, Carpinteria, CA, USA). Finally, the sections were counterstained with Mayer's hematoxylin, dehydrated and mounted.

Microscope slides were scanned with Pannoramic 250 or 1000 Flash digital slide scanner (3DHISTECH Ltd., Budapest, Hungary) with Plan-Apochromat objective, with 20x/0.8 magnification with a resolution of 0.24 µm/pixel. WSIs were visualized

using Caseviewer software version 2.3 or 2.4. (3DHISTECH Ltd). The image quality was ensured by the automatic scanner initialization and visual inspection after scanning (ie, verifying that the images are in focus and no artefacts are present).

4.4 Electron microscopy (III)

The TEM sample preparation was performed in the Laboratory of Electron Microscopy in the Institute of Biomedicine, in the University of Turku. Liver tissue was cut to 1mm x 1mm pieces, samples were fixed with 5% glutaraldehyde s-collidine buffer, postfixed with 1% OsO_4 containing 1.5% potassium ferrocyanide, dehydrated with ethanol and flat embedded in 45359 Fluka Epoxy Embedding Medium kit. Thin sections were cut with an EM UC7 (Leica Microsystems GmbH) ultramicrotome to a thickness of 70 nm. Sections were collected on 200 Mesh copper grids coated with carbon-stabilized formvar film (product number 01801, Ted Pella inc.) The sections were stained with 1% uranyl acetate and 0.3% lead citrate. The sections were examined with a JEM-1400 Plus transmission electron microscope (JEOL ltd.) operated at 80 kV acceleration voltage with objective lens aperture of 60 µm and resolution of 0.69 nm/pixel. Images were recorded with Quemesa camera (EMSIS GmbH).

The peroxisomes were imaged with 20000x magnification with a resolution of 0.69 nm/pixel. To analyze the size of peroxisomes in TEM images, Fiji (ImageJ) (Schindelin et al., 2012) was used to measure the area of each peroxisome. The analysis of CTRL Chow group covered two samples including analysis of 40 images containing all together 60 peroxisomes. The analysis of KO Chow group covered three samples including analysis of 49 images containing all together 95 peroxisomes.

4.5 RNA extraction and transcriptome analysis (II & III)

Total RNA was extracted from frozen liver tissues using TRIsure™ (Bioline, London, UK) and DNase-treated using a DNase I kit (Sigma-Aldrich, Saint Louis, MO, USA). RNA was reverse transcribed using SensiFAST™ cDNA Synthesis kit (Bioline) and RT-qPCR analysis was performed using Sybr Green kit (Thermo Fisher Scientific, Waltham, MA, USA) and analyzed using Bio-Rad CFX96 Real-Time PCR Detection System (Bio-Rad, Hercules, CA, USA) combined with CFX Manager software (Bio-Rad). RNA sequencing of total RNA was performed using an Illumina NovaSeq 6000 Sequencing System (Illumina, San Diego, CA, USA) at Novogene (Cambridge, UK). The sequencing length was 150 base pairs from both ends and the sequencing depth was 20 million reads per sample. The read quality

was checked with FastQC and the reads were aligned to mm10 and assigned to genes with Rsubread. EdgeR was used for normalization to counts per million (CPM) and ROTS for the differential expression (DE) analysis.

In publication **II**, DE genes with FDR <0.05 and absolute fold change (FC) >2.0 were selected for functional enrichment analysis using Metascape (metascape.org) with default functional categories from GO Biological Processes (GO), KEGG (K) and Reactome (R). Additional enrichment analysis was done using the DisGeNET database.

In the manuscript **III**, transcriptomic data were analyzed using the Chipster software platform for high-throughput data processing. Raw sequencing files were aligned to the *Mus musculus* reference genome (GRCm39) using Hisat2 (v2.0.5). Gene-level counts were generated with the HTSeq quantification tool, and differential gene expression was assessed using DESeq2. Gene ontology (GO) enrichment analysis of attained differentially expressed genes was performed using the Database for Annotation, Visualization and Integrated Discovery (DAVID) (Huang et al., 2009; Sherman et al., 2022). To visualize the data Sankey plot and waterfall plot was generated by SRplot (https://www.bioinformatics.com.cn/srplot).

4.6 Image analysis methods

Image analysis workflows developed are part of the results of the present study and are discussed in more details under the chapter 5.1.

4.6.1 Deep-learning method to quantitate micro- and macrovesicular steatosis (I, II and III)

Hepatic steatosis was quantified from digitized whole slide images (WSIs) of HE-stained liver sections with a computerized, deep learning-based, method created in the Aiforia Create (version 5.3, Aiforia Technologies, Helsinki, Finland). The AI model creation workflow encompassed both training and validation phases. The model development started with labeling the training data that included all together 101 whole slide images from mouse models, which had been previously characterized to present with liver steatosis. This data included HE-stained WSIs of formalin-fixed, paraffin-embedded mouse liver samples from 9-month–old mice deficient in hydroxysteroid (17β) dehydrogenase 13 (Adam et al., 2018) or deficient in hydroxysteroid (17β) dehydrogenase 12 (Heikelä et al., 2020) and their wild-type littermates in C57Bl6; 129S5 hybrid (50/50) and C57BL/6NCrl genetic background, respectively. In addition, the training data included HE-stained WSIs of mouse liver samples obtained from C57Bl wild-type mice kept on a Western diet (D12079B; Research Diets Inc., New Brunswick, NJ) for 14 weeks. Validation data included 20

HE-stained WSIs of mouse liver samples from wild-type mice with C57Bl6; 129 hybrid genetic background and mice with same background kept in high-fat diet (HFD) conditions (D17010103; Research Diets Inc.) for 12 weeks.

The representative areas of morphological features were visually annotated and the training areas and feature labels were manually drawn by one person. The AI model was trained based on these annotations and resulting model was evaluated visually. Based on the evaluation of these AI model results old annotations were edited, and new annotations were created, followed by a new training round. First the model was trained to detect liver parenchyma, including normal hepatocytes, macrovesicular hepatocytes and microvesicular hepatocytes. This algorithm excludes background, holes in the tissue, blood vessels and other features that do not belong to the liver parenchyma. Next, the second algorithm was trained to recognize micro- and macrovesicular steatosis in the hepatocytes, and eventually these two were combined. The slides to be analysed were uploaded to Aiforia cloud and were analysed as batch.

4.6.2 Image analysis workflow to study apoptosis and proliferation in histology (II)

For TUNEL and Ki-67 analyses, the QuPath open-source software platform (version 0.2.0 and 0.6.0) was used (Bankhead et al., 2017). The digital whole slide images (WSIs) were converted to mrxl image format readable by QuPath version 0.2.0. Version 0.6.0 did not require image conversion. Apoptosis and cell proliferation were quantitated using the feature of the positive cell detection, where parameters were set to detect optimally both the Hematoxylin-stained nuclei and IHC stained cells. The proportion of positive cells of all cells was calculated. The analysis was performed to the whole area of four tissue slices on each slide and the workflow was automated to enable effective analysis of the whole dataset.

4.6.3 Image analysis workflow to quantitate liver fibrosis (III)

An automated image analysis workflow to quantify fibrosis in picro sirius-stained (PSR) mouse liver WSIs was created in QuPath software (version 0.2.0 and 0.6.0). The created workflow to detect and quantify fibrosis was based on pixel classification and area quantification. To segment the PSR stains representing collagen, the stain vectors were first set to separate different colours into different image layers. The method is based on color deconvolution (Ruifrok & Johnston, 2001) where stains are digitally separated from a color image. Two threshold-based pixel classifiers for segmenting the liver tissue and the fibrotic tissue were created. The Parenchyma classifier detects the tissue on the slide and creates annotations, and

after that excludes the artefactual edge staining from the annotation areas. The Fibrosis classifier detects the fibrosis within the annotated tissue area. The parameters of the Fibrosis classifier were optimized by comparing the detection of the classifier to visual histological evaluation of fibrosis in representative areas.

The created classifiers were applied to different datasets. Every image data set was analyzed in individual QuPath project, where the command -based workflow was used to create a script to automatize the workflow for the analysis of large datasets. Before exporting the resulting measurements to an output file, each WSI was visually inspected and arisen incorrect parenchyma segmentations and annotations were deleted or corrected manually by using the wand or brush tool. The fibrosis percentage of each section was calculated by dividing the area of fibrosis (μm^2) by the total tissue area (μm^2).

4.6.4 Liver micro-ultrasound image analysis (III)

Five mice from each experimental group were randomly selected for micro-ultrasound imaging. Prior to imaging, each mouse was anesthetized using 3% isoflurane (in 1l/min of oxygen) in an induction chamber connected with a scavenger cannister. After induction, the mouse was positioned supine on a temperature-controlled board at 36°C, with its limbs stretched out and secured in a way that minimized motion during the scan. Anaesthesia was maintained throughout the procedure via a nose cone delivering 1.5% isoflurane. To prepare the imaging site, abdominal hair was removed using an animal hair clipper followed by depilatory cream. A warm acoustic coupling gel (Eco Supergel, Ceracarta, Forlì, Italy) was applied to the abdomen. Imaging was performed using a 40 MHz probe (MX550D) mounted on a mechanical arm and connected to a high-frequency micro-ultrasound system (Vevo 2100, VisualSonics Inc., Toronto, Canada). B-mode ultrasound scans were acquired in a longitudinal orientation, capturing both the medial lobe of the liver and the right kidney within the same image plane and at equivalent depth.

For each mouse, three B-mode images were obtained and analyzed to calculate the hepatic-renal (H/R) echogenicity ratio using ImageJ software. A region of interest (ROI) was drawn on the liver parenchyma as well as on corresponding portion of the renal cortex. These two ROI were drawn at the same depth for both organs and as close to the center of the image as possible in order to ensure similar echo intensity attenuation for both regions and avoid borderline echo distortion. The mean grayscale intensity of the hepatic ROIs was averaged across the three images to yield a single hepatic value per mouse. The same method was applied to the renal ROIs. The H/R ratio was then calculated by dividing the mean hepatic intensity by the mean renal intensity. This ratio serves as an indicator of hepatic fat accumulation, based on the principle that increased liver fat content enhances echogenicity,

resulting in a brighter liver appearance relative to the adjacent kidney and a correspondingly higher H/R ratio.

Table 1. Summary of the image analysis methods.

Imaging method	Image analysis method	Data	What is analysed?	Software used	Publication/ manuscript
Histology	Deep-learning based image analysis	HE stained mouse liver	Micro- and macrovesicular steatosis	Aiforia (commercial)	I, II, III
	Cell detection	Ki-67 and TUNEL stained mouse liver	Cell proliferation and apoptosis	QuPath (open-source)	II
	Area quantification	PSR -stained mouse liver	Fibrosis	QuPath (open-source)	III
Micro-ultrasound	Measuring mean intensity in ROI	B-mode images of liver and kidney parenchyma	Liver steatosis	Fiji (ImageJ) (open-source)	III
Transmission electron microscopy	Measuring area of annotation	TEM images taken with 20000x magnification	Peroxisome size	Fiji (ImageJ) (open-source)	III

4.7 Statistical analysis

Statistical analysis was carried out using GraphPad Prism 10.4.1 software (GraphPad Software, Boston, USA). Shapiro-Wilk test was used to test for normal distribution of the data, and statistical test was chosen depending on the result of the test for normality. Unpaired t-test or Mann-Whitney test was used to determine the statistical significance between two groups at single time point, and two-way ANOVA for multiple time points. Pearson correlation coefficient (r) was used for the correlation analysis. The threshold for statistical significance was set at $p < 0.05$. Results were expressed as mean ± SD.

5 Results

5.1 Image analysis workflows to analyze biomarkers of MAFLD and MASH

The development of MASLD in the hepatocyte-specific HSD17B12KO mice was studied with a wide range of imaging modalities, including quantitative micro-ultrasound, electron microscopy and deep-learning based and conventional histological image analysis. This chapter discusses about image analysis workflows developed and applied and the biological findings justified with image analysis.

5.1.1 Deep-learning based algorithm detects and quantifies micro- and macrovesicular steatosis with high precision and sensitivity

The deep-learning based image analysis for quantifying liver steatosis on histological images of preclinical mouse models for MASLD (previously NAFLD) was created. The AI model detected parenchymal tissue and excluded the white background, fixation artefacts, and vessel structures with convolutional neural network (CNN) 1 (**I**, Fig. 1C, D). The CNN2 of the model accurately detected and quantified the area of tissue containing microvesicular or macrovesicular steatosis (**I**, Fig. 1E, F). The AI model enables the analysis of a whole slide image (**I**, Fig. 1G, H).

The validation of the AI model included utilizing the verification tool in the Aiforia Create, pathologists' evaluation of validation data and comparing image analysis results to other steatosis biomarkers. The results by the verification tool indicated that the model learned the ground truth with high precision (>98%) and sensitivity (>99%) (**I**, Table 1). One pathologist performed pixel level validation, against which the sensitivity of the model was 97% and precision was 89% with total area error of 8.39% (**I**, Supplemental Table S3). Two other pathologists evaluated visually the proportion of cells containing microvesicular or macrovesicular steatosis in validation samples and further, the performance of the AI model was compared to the pathologists´ staging. A strong positive correlation was observed between the image analysis and the pathologists' evaluation of both macrovesicular steatosis and microvesicular steatosis (**I**, Fig. 2A-F). Importantly, the image analysis results performed by the DL model correlated well with

the triglyceride concentration measurement in liver homogenate (**I**, Fig 3C), and with the liver fat content analyzed by an EchoMRI *ex vivo* (**I**, Fig 3D).

5.1.2 Positive cell detection quantifies apoptosis and proliferation

In our studies (Heikelä et al., 2020, 2024) liver damage and growth capacity was investigated by quantification of apoptotic cells and cell proliferation, respectively, in LiB12cKO mice on chow diet. IHC stained mouse liver images were analyzed with positive cell detection in QuPath software. The analysis pipeline included image type definition, segmentation of Hematoxylin-stained nuclei and IHC stained cells. The detection of positive cells and nuclei was optimized by adjusting the parameters until the segmentation result was satisfactory by visual inspection. The optimization included e.g. adjusting the threshold to define cell boundaries accurately and fine-tuning of Sigma/Median filter radius to handle noise or clustered cells. The created classifier was saved and the same classifier was used for images to ensure the data comparability. The proportion of positive cells of all cells was then calculated (**II**, Fig. S2G, H). The analysis was performed to the whole area of four tissue serial sections on each slide and the workflow was automated to enable effective analysis of the whole dataset (**II**, Fig. S2I, J).

Quantification of apoptotic cells by TUNEL staining and image analysis showed a significantly higher percentage of apoptotic hepatocytes in LiB12cKO males compared with WT males at the ages of 6 and 8 months ($FC = 15.7$, $p = .008$ and $FC = 44.4$, $p = .022$), while in 2-month-old females, such difference was not observed (**II**, Fig. 3A, B).

Quantification of proliferative cells by Ki-67 staining and image analysis in LiB12cKO mice showed a significantly higher percentage of hepatocytes positive for immunohistochemical staining for Ki-67 in males in all age groups (2 months: $FC = 2.64$, $p = .006$; 6 months: $FC = 2.81$, $p \leq .001$; 8 months: $FC = 2.89$, $p \leq .001$) and in 2-month-old females ($FC = 1.86$, $p = .008$), indicating an increased hepatocyte proliferation at the age of 2 months onwards (**II**, Fig. 3C, 2D). This suggests the activation of the regenerative pathway in response to hepatocyte damage in the LiB12cKO mice.

5.1.3 Area quantification measures fibrosis

The automated image analysis workflow for quantifying liver fibrosis on histological images was created to study the development from MASLD to MASH in preclinical mouse models. Fibrosis detection and quantification were performed using a pixel classification-based workflow in QuPath software. Two classifiers were established: one for segmenting liver parenchyma and another for identifying fibrotic regions. The parenchyma classifier, optimized for low-resolution tissue-background separation,

defined the tissue area, while the fibrosis classifier, applied at high resolution, was calibrated against expert histological evaluation to ensure accuracy. Stain vector separation was employed to isolate relevant color channels in PSR stained mouse liver images, with representative regions selected to include both fibrosis and parenchyma while excluding background. The analysis pipeline included image type definition, tissue segmentation, object creation, and edge artifact removal. Fibrotic areas were then segmented within the refined tissue annotations, and area measurements were extracted. The fibrosis percentage was calculated as the ratio of fibrotic area to total tissue area and the workflow was scripted and batch-applied to WSI datasets.

The workflow was validated correlating the image analysis-based fibrosis measurements with Col1a1 and Col3a1 gene expression in Hsd17b13KO (n=6) and WT (n=11) male mice on CDAHFD diet for 12 weeks and WT male mice on Chow-diet (n=10) for 12 weeks. The fibrosis measurements were conducted by applying the created image analysis workflow without area exclusion and the RNA sequencing measurements were performed from the same mice. The correlation between measured fibrosis from images and Col1a1 and Col3a1 expression in the liver was statistically significant (p<.001) (Figure 6).

The fibrosis quantification method was applied to study the LiB12cKO mice. Interestingly, KO mice had more fibrosis than WT mice both on HFD and Chow (**III**, Fig. 3B, C).

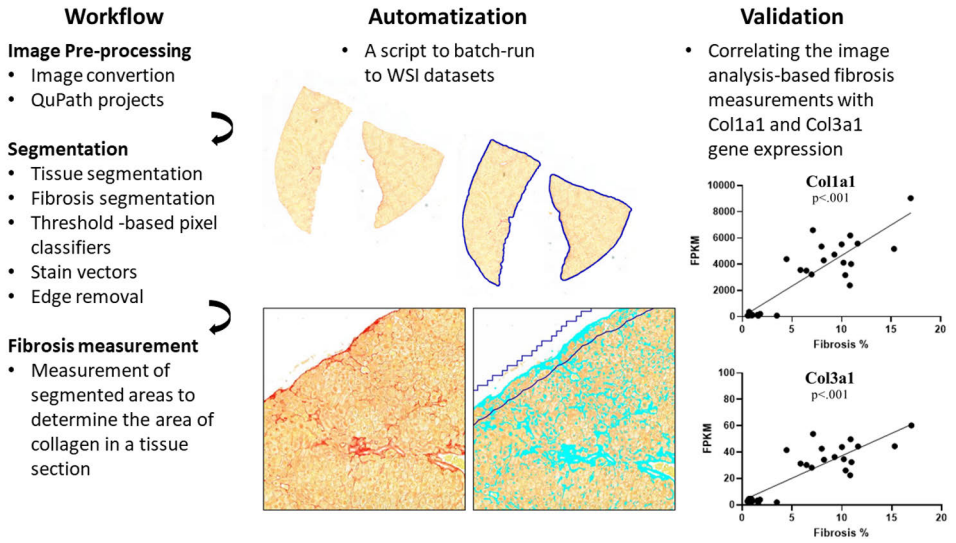

Figure 6. The workflow included the measurement of Picro Sirius -stained area and the parenchyma area to calculate the fibrosis percentage. The workflow was scripted and batch-applied to WSI datasets. In validation phase, the statistically significant correlation between fibrosis and Col1a1 and Col3a1 expression in WT and KO male mice on 12-week CDAHFD diet and WT male mice on Chow diet for 12 weeks was found.

5.1.4 Micro-ultrasound method to measure fat accumulation

The micro-ultrasound method to measure fat accumulation was established in our laboratory, to measure the fat accumulation in the liver over time. The longitudinal micro-ultrasound assessment -method by Di Lascio et al. (Di Lascio et al., 2018) was applied where appropriate and method was optimized for our use.

The liver-specific knockout mice (LiB12cKO) and WT mice were studied on chow and HFD (n=5/group). Ultrasound B-mode images (three per sample, longitudinal view) were analyzed using ImageJ to calculate the Hepatic–Renal (H/R) ratio (Di Lascio et al., 2018). Regions of interest (ROIs) were drawn on the liver parenchyma and renal cortex at the same depth and near the image center to minimize echo distortion (Figure 7). Mean grey intensities from three images per mouse were averaged for both liver and kidney ROIs. The H/R ratio was then calculated by dividing the hepatic by the renal value. The results indicate no difference between genotypes in hepatic-renal ratio measured with ultrasound on chow or HFD (**III**, Fig. 2D). Triglyceride measurements are aligned with the ultrasound result (**III**, Fig. 2B). However, higher intensity was measured on HDF both in WT and KO groups compared to mice on chow diet.

Although no difference between genotypes was observed, a more pronounced difference due to diet was seen, making this method well suited as a non-invasive method to monitor the fat accumulation in the liver in diet intervention experiments on mice.

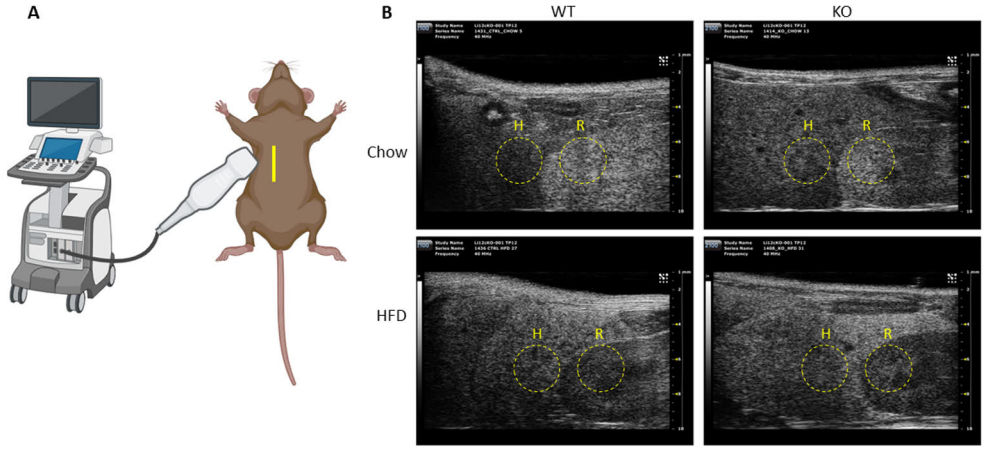

Figure 7. (A) Micro-ultrasound imaging device was used to capture B-mode images (longitudinal view) showing liver parenchyma of median lobe and kidney. (B) In ImageJ software, regions of interest (ROIs) were drawn on the liver parenchyma (H) and renal cortex (R) at the same depth and near the image center to minimize echo distortion. Mean grey intensities from three images per mouse were averaged for both liver and kidney ROIs. The H/R ratio was then calculated by dividing the hepatic by the renal value. HFD: High fat diet.

5.2 The role of the HSD17B12 in the fat metabolism and liver function

5.2.1 The HSD17B12 mice are resistant to weight gain

The LiB12cKO mice showed no differences in body weight or composition compared to wild-type controls at 2 months of age on chow diet. However, by 6 and 8 months, their body weight was significantly reduced relative to age-matched WT mice (**II**, Fig. 1A). Interestingly, after 12 weeks on HFD, LiB12cKO mice did not gain weight similarly as the control mice, and the weight of LiB12cKO mice on HFD did not differ from the KO mice on chow diet (**III**, Fig. 1A).

Body composition analysis showed significantly lower body fat in 6-month-old LiB12cKO females (FC = −1.57, p = .010), but not in males on chow diet. By 8 months, both sexes had reduced fat percentages compared to controls (males: FC = −1.34, p = 0.028; females: FC = −1.63, p ≤ .001) (**II**, Fig. 1B). Lean mass was unchanged in females at both time points and in 8-month-old males, though 6-month-old LiB12cKO males showed a slight reduction on chow diet (FC = −1.07, p = 0.023) (**II**, Fig. 1C). Accordingly, on HFD, the body composition analysis revealed that the weight gain was exclusively due to increased fat mass in WT mice (**III**, Fig. 1D, E). Supported by the ex vivo measurement of amount of gonadal fat, there is less fat in LiB12cKO mice than in controls on HFD (**III**, Fig. 1F and 1G).

The findings cannot be explained by changes in appetite. On chow diet, there was no difference in the food intake between the LiB12cKO and the WT mice (**III**, Fig. 1C), even though the body weight was reduced in KOs. Surprisingly, LiB12cKO mice on HFD were eating more than WT mice on HFD (**III**. Fig. 1C), although the body fat content was decreased.

5.2.2 The HSD17B12 deficiency alters the lipid droplet formation

On chow diet, both male and female LiB12cKO mice exhibited significantly enlarged livers compared to wild-type (WT) controls across all age groups studied (**II**, Fig. 1F). This enlargement was already evident at 2 months of age (males: FC = 2.11, p ≤ .001; females: FC = 1.57, p = .001), became more pronounced by 6 months (males: FC = 2.31, p ≤ .001; females: FC = 1.65, p = .002), and remained significant at 8 months (males: FC = 1.51, p = .001; females: FC = 1.64, p ≤ .001). Notably, the livers of 2-month-old LiB12cKO mice appeared pale, a feature that often indicates the appearance of fatty liver (**II**, Fig. 1G). Histological analysis with HE staining confirmed the presence of lipid droplets (LDs) in LiB12cKO livers as

early as 2 months, with this phenotype persisting throughout the study period (**II**, Fig. 2A).

Interestingly, on HFD there were no difference in liver size between KOs and WT, even though KO livers were larger on chow diet (**III**, Fig. 2A). There was no difference between genotypes in hepatic-renal ratio measured with ultrasound (**III**, Fig 2D) and triglyceride measurements (**III**, Fig. 2B), but both are higher in mice fed with HFD.

Micro- and macrovesicular steatosis was quantified by the developed deep learning-based model for quantifying hepatic steatosis. The capacity of the algorithm to accurately differentiate between microvesicular and macrovesicular steatosis emerged as a critical feature in the analysis of the HSD17B12 mouse model. This distinction enabled us to identify disablement in lipid droplet expansion associated with hepatocyte-specific disruption of the *HSD17B12* gene, suggesting a mechanistic link between gene function and lipid metabolism. Markedly higher areas of microvesicular steatosis were identified in LiB12cKO male liver already at the age of 2 months compared with WTs (**II**, Fig. 2B). This difference between the genotypes remained throughout the 8-month-long study period (FC = 7.60, $p = 0.0015$ at 2 months of age; FC = 18.74, $p = 0.0012$, at 6 months of age). The dynamics were different in the females, as there was no difference between the genotypes in the 2- and 6-month-old mice, but at 8-month-old LiB12cKO females, the areas with microvesicular steatosis were highly increased (FC = 4.25, $p = 0.0007$). Furthermore, the formation of macrovesicular steatosis was hindered in LiB12cKO males, resulting in an increased ratio of microsteatosis/macrosteatosis in the LiB12cKO mice (**II**, Fig. 2B).

Surprisingly, on HFD, histological image analysis indicated that LiB12cKO mice develop less macro- and microvesicular steatosis (**III**, Fig. 2F, G) compared to controls. The histological image analysis of steatosis was confirmed with pathologist evaluation, according to which LiB12cKO mice on HFD show increased lipidosis, but clearly less than in WT mice (**III**, Fig. 2H)

At 2 months, LiB12cKO male mice showed elevated levels of most lipid classes, notably cholesterol ester (CE) (FC = 10.72), lactosylceramide (LCER) (FC = 5.86), and triacylglycerol (TAG) (FC = 4.09), which are key neutral lipids in LDs and likely contribute to the observed microsteatosis (**II**, Fig. 2C). Interestingly, only sphingomyelin (SM) levels were reduced (FC = −1.45) (**II**, Fig. 2C). Principal component analysis clearly separated LiB12cKO and control mice based on lipid profiles (**II**, Fig. S3). Smpd3 expression, which encodes an enzyme that breaks down SM into ceramide (CER) and phosphatidylcholine (PC), was 8.5-fold higher in LiB12cKO livers, aligning with the SM decrease. Despite that the amount of visible microvesicular steatosis was higher in the LiB12cKO livers, major LD monolayer

lipids (PC and phosphatidylethanolamine (PE)) were only moderately increased or unchanged.

Interestingly, the RNA sequencing data showed differences in CIDEC and Flot1 between CTRL and LiB12cKO mice (**II**, Fig. 2G). Flot1 is a LD-associated protein that facilitates the interactions between LDs and endoplasmic reticulum and interestingly, the expression of Flot1 was increased in LiB12cKO mice. CIDEC is a lipid transfer protein and it is involved in lipid droplet enlargement. The increase in the CIDEC expression further supported the deficiency in LD expansion in the LiB12cKO liver. Notably, many major urinary proteins were strongly downregulated in LiB12cKO livers, indicating possible ER stress as an early response to HSD17B12 deficiency. These findings suggest that LD formation is disrupted by *Hsd17b12* loss in hepatocytes.

After HFD, RNA sequencing analysis revealed major differences in the transcriptomes between WT and the LiB12cKO mice with over 1600 significantly altered transcripts, with close to 110 transcripts altered more than 16-fold. These included many genes with being almost non-detectable in WT but with significant expression in the LiB12cKO mice. While a deeper analysis of the transcriptomic alterations is to carried out, we identified marked up-regulation of transcripts coding for proteins involved in intracellular vesicle transportation, e.g., (DYNC1I1, KIF1A, PLEKHD1, and TBC1D21) (**III**, Fig. 3D, F). This is line with the identified defect in lipid droplet expansion that is expected to suppress the formation of intracellular vesicles and their exocytosis. The altered lipid metabolism with increased oxidative stress is also the likely reason for a strong up-regulation of glutathione peroxidase 2 (GPX2) and Gamma-Glutamyltransferase 1 (GGT1) in LiB12cKO mice fed with HFD (**III**, Fig. 3G). Of the down-regulated transcripts we are currently highly excited about the drastic suppression of Complement factor D (CFD, also) as its function has been shown to act as an adipokine (**III**, Fig. 3H).

5.2.3 The HSD17B12 deficiency causes liver damage

The amount of liver damage associated marker alanine aminotransferase (ALT) enzyme was increased in the serum of LiB12cKO mice on chow diet (**II**, Table 2, **III**, Fig. 3A) and in mice on HFD (**III**, Fig. 3A). Liver damage was indicated also by the quantification of apoptotic cells by TUNEL staining, showing a significantly higher percentage of apoptotic hepatocytes in LiB12cKO males compared with WT males on chow diet (**II**, Fig. 3A, B). The results also showed a significantly higher percentage of hepatocytes positive for immunohistochemical staining for Ki-67 in males in all age groups on chow diet indicating an increased hepatocyte proliferation at the age of 2 months onwards on chow diet (**II**, Fig. 3C, D). This suggests the activation of the regenerative pathway in response to hepatocyte damage in the

LiB12cKO mice. Interestingly, signs of a relevant hepatic inflammation were not observed in any age group of either sex on chow diet.

The visual inspection of HE stained images of LiB12cKO mice on chow diet indicated pronounced hepatocellular hypertrophy with marked anisokaryosis, cytoplasmic invagination and occasional mitotic figures (**II**, Fig. 3E, F). Given the observation of cellular hypertrophy, we aimed to investigate whether this phenotype is associated with alterations in peroxisomal structure or function. Peroxisomes appeared morphologically unaltered, with no observable differences in their abundance, distribution, or structure between experimental groups. The peroxisomes were visualized with TEM with 20000x magnification and the area of 155 peroxisomes was measured and analyzed. The analysis of WT Chow group covered two samples including analysis of 40 images containing all together 60 peroxisomes. The analysis of KO Chow group covered three samples including analysis of 49 images containing all together 95 peroxisomes. No statistically significant difference in peroxisome size between KOs and WTs was found (Figure 8).

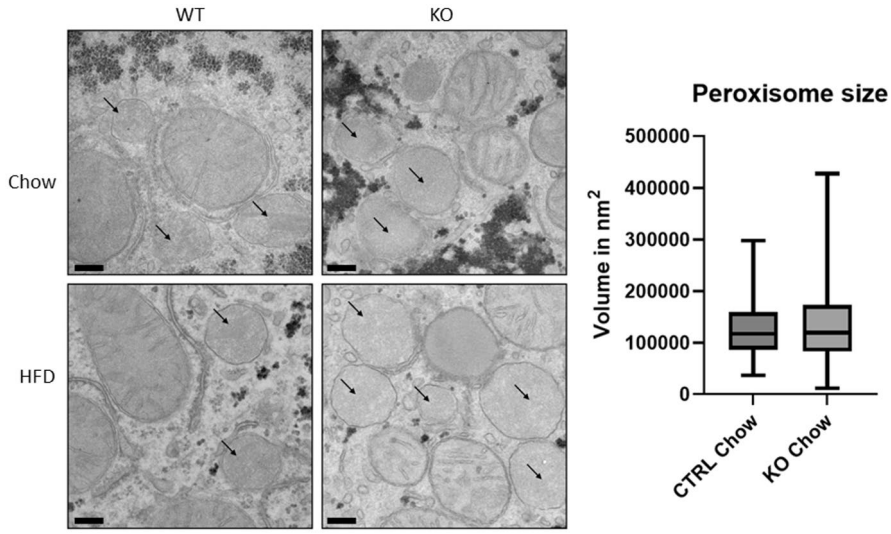

Figure 8. Representative images of hepatocyte peroxisomes (arrows). Scale bar 2 µm. No statistically significant difference in peroxisome size between LiB12cKO mice and WTs was found.

Interestingly, the TEM imaging revealed the atypical shape of hepatocyte nuclei in KO mice. The nuclear envelope is uneven, it blebs and invaginations are found (Figure 9).

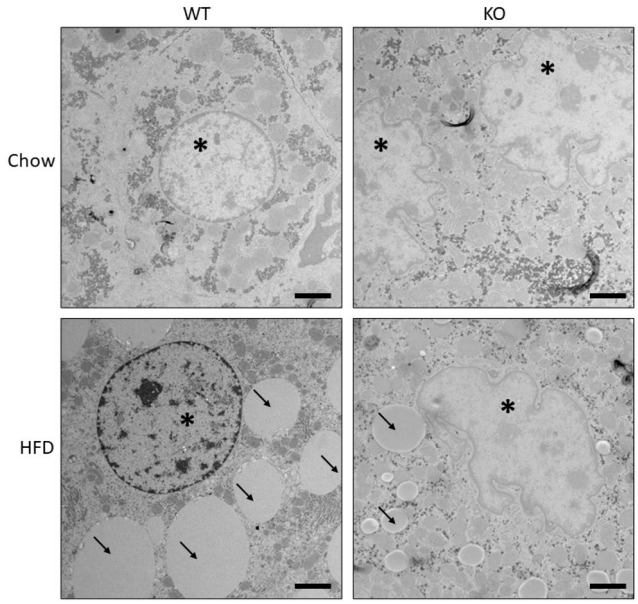

Figure 9. Representative images of hepatocyte nuclei. Asterisk nucleus, arrow lipid droplets. Scale bar 2 µm.

6 Discussion

This PhD work integrates two primary themes: a methodological focus on image analysis and a biological investigation of HSD17B12 biology, especially in the liver. The image analysis framework was developed to enable the quantitative assessment of features associated with the progression of MASLD and MASH. By applying advanced computational techniques, the framework facilitates the detection and quantification of key biomarkers across different disease stages, offering a comprehensive toolkit for characterizing liver pathology in preclinical models.

6.1 Image analysis workflows to analyze biomarkers of MAFLD and MASH

6.1.1 Histological analysis of MAFLD and MASH

The deep-learning (DL) -based image analysis model was developed to automatically quantify microvesicular and macrovesicular steatosis in HE-stained mouse liver sections with high precision and sensitivity. The aim was to create a generic model, that would allow the analysis of data originating from different mouse models and different research laboratories. The model was trained on both genetically modified and diet-induced MASLD mouse models, enhancing its versatility. The model showed strong agreement with expert pathologist assessments and biochemical validations, including EchoMRI and triglyceride measurements. Unlike previous pre
clinical methods (Ramot et al., 2020; Sethunath et al., 2018), it quantifies steatosis by tissue area rather than individual lipid droplets, aligning better with existing scoring systems (Kleiner et al., 2005; W. Liang et al., 2014).

The DL model is notable for its ability to detect microvesicular steatosis, a key marker of hepatotoxicity (Jaeschke, 2002; Kleiner et al., 2014), and visualize its spatial distribution. Prior work in developing deep learning models to detect fat accumulation in the liver has concentrated on segmenting and quantifying macrovesicular lipid droplets (Guo et al., 2019; Roy et al., 2020) However, there has been less attention on developing methods to quantify microvesicular steatosis,

although a few automatic methods have been published (Ramot et al., 2020). The task of quantifying microvesicular steatosis poses a challenge for automated image analysis, because the size and shape of lipid droplets vary and the discrimination of microvesicular steatosis from general ballooning is challenging (Farrell et al., 2019). However, quantifying both microvesicular and macrovesicular steatosis is essential to better define the stage of the steatosis in the experimental models.

In this study, a deep learning -based image analysis method was applied when appropriate, but in addition many conventional methods were also applied. Steatosis is one of the most studied features in HE stained mouse liver samples. In paraffin sections, the fat is dissolved during tissue processing, and therefore, can be confused with other white features, such as holes and glycogen, in image analysis. Therefore, deep-learning was used in the first project. In the following projects, the feature to be analyzed was clearer, since there was specific staining for the feature to be analyzed (fibrosis, apoptosis, proliferation). Therefore, conventional methods were appropriate. The deep-learning methods has exploded in all applications, but it has also downsides. Training large AI models requires massive computational power, often using energy-intensive data centers and these data centers use millions of liters of water annually for cooling systems (Schwartz et al., 2019; Strubell et al., 2019). Thus, for research questions of limited complexity, the application of conventional image analysis techniques remains methodologically appropriate and computationally efficient.

Furthermore, the internal decision-making mechanisms of deep neural networks are inherently opaque and difficult to interpret in a human-understandable manner (black box -problem), which has led to the emergence of explainable artificial intelligence (XAI) as a prominent area of research (Evans et al., 2022). Deep learning-based image editing is now a common feature in consumer technology. For example, smartphones often suggest edits such as removing background individuals from photos. Although such tools are not yet standard in scientific research workflows, they are likely to become integrated over time. This shift underscores the importance of maintaining a critical approach: researchers must actively evaluate and guide AI-generated outputs, rather than adopting algorithmic suggestions without review. Preserving scientific rigor and interpretability depends on treating AI as a supportive tool rather than an autonomous decision-maker.

The methodological emphasis of this research lies in the domain of histological image analysis. While the foundational principles of computational image analysis are broadly applicable, histopathology presents unique domain-specific challenges that continue to pose difficulties for researchers. One such challenge arises from the nature of WSI. When histological slides are digitized using whole-slide scanners, the resulting image formats are typically defined by the manufacturer of the scanner. Although basic visualization and processing tools are often provided, researchers

aiming to perform advanced image analysis using third-party software must ensure compatibility with these formats. Some researchers are content to analyze a certain number of representative snapshots instead of facing the challenges posed by large-scale images. But obviously, the WSI format provides more comprehensive results. The Digital Imaging and Communications in Medicine (DICOM) standard format is used for storing, transmitting, and handling imaging data, but its wider uptake in histopathology has been slow, because histological images are multi-layered and multi-scale, which DICOM was not initially designed to handle (Clunie, 2021). In this work, both commercial and free open-source software were used, but in both systems, WSIs needed to be converted to suitable format to be opened in the software. Image conversion is an extra step in analysis workflow that consumes time and computing power.

One essential feature of histological images is colors, and color normalization is often needed. However, in this work, no color normalization methods were used. In deep learning-based method, the idea was to train the model with versatile data from different research groups to ensure the wide applicability of the algorithm. Another approach would have been forcing the data to certain color frame beforehand. In this work, when applying conventional image analysis workflows, the histological sample preparation and staining was coherent, and color variation was minimized by that. The samples to be compared were always processed from start to finish in exactly the same way, under the same conditions and at the same time.

QuPath is an open source software commonly used for research in digital pathology, because it offers a set of tools for working with whole slide images (Bankhead et al., 2017). The positive cell detection -feature is a built-in algorithm in QuPath and it was used to quantify apoptosis and proliferation in IHC stained images. The parameters included intensity and morphology parameters for nuclei and positive cells, and parameters were optimized to detect optimally both the Hematoxylin-stained nuclei and IHC stained cells. Of course, the set parameters and threshold values affect the number of detected objects, but therefore, all images were analyzed similarly and the relative differences between sample groups were compared instead of looking at the actual values. Quantification of apoptotic cells by TUNEL staining and image analysis showed a significantly higher percentage of apoptotic hepatocytes in LiB12cKO males compared with WT males. In addition, quantification of proliferative cells by Ki-67 staining and image analysis in LiB12cKO mice showed a significantly higher percentage of hepatocytes positive for immunohistochemical staining for Ki-67 in males in all age groups indicating an increased hepatocyte proliferation at the age of 2 months onwards. In this workflow, one threshold value was defined to classify pixels as belonging either to an object/area or background. Technically it is possible to set many thresholds and grade IHC-stained images, as in pathology often relevant, but setting one threshold

value is more ethical when considering the fact that the darkness of stain does not directly equate to the amount of expression of a given antigen.

For fibrosis detection and quantification, a pixel classification-based workflow was created in QuPath. The extent of fibrosis in PSR-stained mouse liver samples was quantified and compared to the expression levels of collagen-related genes (Col1a1 and Col3a1). A statistically significant correlation was observed between image-derived fibrosis measurements and gene expression levels, supporting the reliability of the image analysis approach. Notably, similar image analysis workflow implemented in other image analysis platform have demonstrated strong correlation with other established methods, such as biochemical assays and traditional histological scoring systems (Serdjebi et al., 2022). CNN based model to measure hepatic fibrosis in mice in PSR stained images has been also developed (Kim et al., 2023). This model provided normalized fibrosis grades and visual annotations of fibrotic areas on WSIs. A well-trained CNN enables scalable and robust image analysis across diverse cases, but its development demands significant computational resources, annotated datasets, and specialized expertise. In contrast, traditional workflows, such as ours, require fewer resources but are limited to narrowly defined scenarios and lack generalizability. Our developed fibrosis quantification workflow was applied to study the LiB12cKO mice. Interestingly, KO mice had more fibrosis than WT mice both on HFD and Chow. This area quantification method does not measure, how dark the staining is, but with one threshold value determines area that is fibrotic. This applies the same idea described above of using one threshold and concentrating on relative differences instead of actual values.

6.1.2 *In vivo* imaging by micro-ultrasound to measure fat accumulation

The micro-ultrasound method to measure fat accumulation in mouse liver was developed. The method is based on the idea of using kidney as a reference organ for liver. Because of the low cost, the absence of radiation exposure and the wide availability, US is often used in screening for MASLD in humans. The accumulation of fat causes the liver to appear hyperechoic compared with the kidney. This finding is nonspecific and does not differentiate fat from other substances such as glycogen (Fitzpatrick, 2014). In our ultrasound results, the intensity of liver is higher in mice on HFD, suggesting the accumulation of fat in the liver. This is in line with triglyceride measurements, but somewhat contradicts with histology. This rises the uncertainty if the finding is fat or something else, like glycogen.

The US methods developed to quantitate fat accumulation in the liver often uses RF-data. However, in this work, the available device did not produce RF-data, so

only images were available for method. In that sense, this work does not include QUS (quantitative ultrasound). The method to measure H/R ratio was applied from work by Faita et al. (Faita et al., 2018) including the exact positioning of probe to visualize liver and kidney similarly in every image. The H/R ratio (referred to as the "steatoscore" in their workflow) was among several ultrasound-derived parameters evaluated. In their study with db/db mice, steatoscore was higher in db/db mice compared to WTs, but the difference did not reach statistical significance (p=0.059), and the authors note that the measurement of the steatoscore represents a pioneering approach in the use of ultrasound-based parameters for assessing hepatic steatosis (Faita et al., 2018). However, in longitudinal study with ob/ob mice, the steatoscore was higher in db/db mice compared to WTs in both time points (Di Lascio et al., 2018).

Based on our studies and literature, micro-ultrasound has limited sensitivity for detecting hepatic changes. It is well-suited for longitudinal monitoring of the effects of diet on the liver of mice, but it cannot distinguish small differences between study groups, nor does it reveal what type of fat accumulates in the liver.

However, 3R is an important principle in all mouse work. The 3R principle stands for Replacement, Reduction, and Refinement and is a foundational ethical framework introduced by Russell and Burch in 1959 to promote humane and scientifically responsible use of animals (Russell & Burch, 1992). Longitudinal *in vivo* methods are needed to reduce the number of animals to be used, and the establishment of this method to measure fat accumulation in mouse liver is step towards using less animals.

6.2 The role of the HSD17B12 in the fat metabolism and liver function

Hsd17b12 is highly expressed in the liver, a key organ in energy metabolism and body weight regulation, in both humans and mice (Heikelä et al., 2020; Sakurai et al., 2006b). Inducible, systemic disruption of HSD17B12 in adult mice led to rapid body weight loss within six days post-induction, accompanied by reduced fat and lean mass, severe dehydration, and ultimately death within a week (Heikelä et al., 2020). These mice also developed microvesicular liver steatosis, underscoring the gene’s critical role in maintaining metabolic homeostasis (Heikelä et al., 2020). To further investigate the metabolic function of HSD17B12, we generated a liver-specific knockout mouse model (LiB12cKO) (Heikelä et al., 2024), which has been utilised in this study.

The study revealed that hepatocyte-specific deletion of HSD17B12 from the fetal stage onward did not reproduce the rapid weight loss or lethality seen in the global inducible knockout. Our findings revealed a progressive and diet-sensitive

phenotype in LiB12cKO mice, characterized by reduced body weight due to reduced adiposity, that becomes evident with age and under metabolic challenge. While no differences in body weight or composition were observed at 2 months, LiB12cKO mice exhibited significantly lower body weight by 6 and 8 months, suggesting a delayed but sustained impact of *Hsd17b12* deletion in hepatocytes on systemic energy balance.

Strikingly, LiB12cKO mice exhibited significantly reduced weight gain on HFD compared to WT controls, despite comparable or even increased food intake, indicating impaired response to dietary fat load. Echo-MRI and *ex vivo* fat analyses confirmed that the reduced weight gain in KO mice on HFD was attributable to decreased fat mass reinforcing the systemic metabolic impact of hepatic Hsd17b12 loss. This phenotype was not observed under chow diet, indicating that the protective effect of HSD17B12 deletion is diet-dependent. These findings highlight a role for hepatocyte-expressed HSD17B12 in regulating whole-body adiposity, though its impact is significantly milder than in systemic knockouts, where multiple tissues are affected (Heikelä et al., 2020).

Recent GWAS studies indicate that HSD17B12 plays a critical role in adipose tissue plasticity and overall metabolic health, including influencing susceptibility to type 2 diabetes (Kulyté et al., 2022). Moreover, HSD17B12 is implicated in pancreatic β-cell function and broader metabolic regulation, reinforcing its potential as a biomarker or therapeutic target for obesity and type 2 diabetes (Hachim et al., 2020).

In LiB12cKO mice, the inability to store excess dietary fat despite normal or elevated caloric intake suggests that HSD17B12 is essential for hepatic lipid metabolism and systemic lipid distribution. This phenotype mirrors features of lean MASLD, where lipid storage is impaired despite sufficient or excessive energy intake. Clinically, patients with lean MASLD may be underdiagnosed due to their non-obese phenotype, but are at high risk for progressive liver disease, including fibrosis and cirrhosis, and cardiometabolic complications (Desai et al., 2025). Globally up to 20% of the patients with MASLD are lean or non-obese (Xu et al., 2022) and similarly to obese MASLD, also lean MASLD is more prevalent in men than in women (Lu et al., 2020).

Our study demonstrates that hepatocyte-specific deletion of Hsd17b12 leads to significant hepatic lipid remodeling and altered liver physiology, even under standard chow diet conditions. Both male and female LiB12cKO mice exhibited enlarged livers as early as 2 months of age, with liver enlargement persisting and intensifying with age. This phenotype was accompanied by pale liver appearance and histologically confirmed microvesicular steatosis, suggesting early and sustained disruption of lipid metabolism.

Interestingly, despite the liver enlargement and steatosis on chow diet, LiB12cKO mice did not show increased liver size or steatosis on high-fat diet (HFD). This paradoxical finding suggests that HSD17B12 deficiency may impair the liver's adaptive response to lipid overload, potentially by limiting lipid droplet (LD) expansion. In accordance with this, deep learning-based histological analysis revealed a marked increase in microvesicular steatosis and a reduction in macrovesicular steatosis in males, indicating a failure in LD maturation. This was further supported by the elevated microsteatosis/macrosteatosis ratio in LiB12cKO livers.

Previous studies by others show, that HSD17B12 depletion *in vitro* leads to a marked reduction in lipid droplet (LD) size, which also impairs virus replication likely due to disrupted formation of membrane-coated viral particles (Mohamed et al., 2020). Since LD formation protect tissues from lipotoxicity (Zadoorian et al., 2023), impaired LD formation may contribute to the liver toxicity observed in LiB12cKO mice, including increased hepatocyte apoptosis and elevated serum ALT and ALP levels, in the presence of only mild steatosis.

Lipidomic profiling revealed accumulation of neutral lipids such as CE, LCER, and TAG in 2-month-old LiB12cKO males, consistent with the observed microsteatosis. Notably, sphingomyelin (SM) levels were reduced, potentially due to upregulation of Smpd3, which encodes sphingomyelin phosphodiesterase (Hofmann et al., 2000). This shift in lipid composition may compromise LD membrane integrity and contribute to impaired LD expansion. Transcriptomic analysis further supported this hypothesis. Increased expression of Flot1, a protein involved in LD–ER interactions, and CIDEC, a key regulator of LD fusion and growth (Lyu et al., 2021), suggests a compensatory response to defective LD expansion. Additionally, the downregulation of major urinary proteins (MUPs) points to endoplasmic reticulum (ER) stress, possibly triggered by disrupted lipid handling in hepatocytes.

Surprisingly, under HFD, LiB12cKO mice exhibited less hepatic steatosis than controls, as confirmed by both automated image analysis and pathologist evaluation. This suggests that HSD17B12 is essential for the liver capacity to store excess lipids, and its absence may limit lipid accumulation despite dietary fat overload.

Our findings reveal that hepatocyte-specific deletion of HSD17B12 leads to a mild liver injury, as evidenced by elevated serum alanine aminotransferase (ALT) levels and increased hepatocyte apoptosis. Although ALT levels showed only a trend toward further elevation under high-fat diet (HFD), the consistent increase across conditions suggests a baseline vulnerability to hepatocellular damage in the absence of HSD17B12.

The TUNEL assay confirmed a significantly higher proportion of apoptotic hepatocytes in LiB12cKO males on chow diet, indicating that cell death is an early

and sustained feature of the phenotype. This was accompanied by a marked increase in Ki-67–positive hepatocytes, suggesting compensatory proliferation and activation of regenerative pathways in response to ongoing liver injury. Notably, despite the cell death and regeneration, no significant hepatic inflammation was observed, indicating a non-inflammatory form of liver damage, which may resemble certain subtypes MASLD or toxic liver injury. However, LiB12cKO mice exhibited a mild increase in hepatic fibrosis on both chow and HFD, as assessed by Picro Sirius Red staining. This suggests that HSD17B12 deficiency predisposes the liver to fibrotic remodeling, independent of steatosis severity. These findings challenge the traditional paradigm linking fibrosis primarily to steatosis and highlight the need to explore non-steatotic pathways of fibrogenesis.

The HE-stained liver sections from LiB12cKO mice exhibited pronounced hepatocellular hypertrophy, anisokaryosis, cytoplasmic invaginations, and occasional mitotic figures. These features are indicative of increased cellular activity and possibly compensatory proliferation (Rozga, 2002). The presence of anisokaryosis and nuclear envelope irregularities, including blebbing and invaginations observed via TEM, further supports the notion of nuclear stress or altered nuclear-cytoplasmic interactions, which may be linked to disrupted lipid metabolism or oxidative stress responses in the absence of HSD17B12 (Bahmanyar & Schlieker, 2020; Kristiani & Kim, 2023).

While the molecular mechanisms behind the observed protection against HFD induced obesogenic insult remains to be studied in detail, transcriptomic analysis of the WT and LiB12cKO mice provided clues for such mechanisms. The most highly up-regulated genes GPX2, GGT1 and some of the other highly up-regulated transcripts code for proteins that are classical targets of Nuclear factor erythroid 2–related factor 2 (NFR2) (Banning et al., 2005), and induced in the presence of high oxidative stress (Colemonts-Vroninks et al., 2020). A strong suppression of our candidate adipokine, CFD, was found in the hepatocytes of LiB12cKO on both chow and HFD. In fact, CFD was the gene of transcript that was the most reduced in the hepatocytes of the LiB12cKO males compared to WT males. The connection between the hypothesized increased oxidative stress is less clear, while CFD has been shown to be a target for PPARγ (Sriboonaied et al., 2025). In human serum CFD is positively correlating with BMI, fat mass and insulin resistance (Milek et al., 2022; Zheng, 2023), and it has been shown to regulate adipocyte differentiation (Song et al., 2016). However, CFD is expected to be mainly produced from the adipocytes, while role of hepatic CFD is less understood. However, CDF KO mice show reduced fat mass and are resistant to diet-induced obesity (Tsuru et al., 2020), similar to the LiB12cKO mice, while deleting HSD17B12 from the adipocytes did not result into adipose tissue loss (Heikelä et al., 2020). CDF KO mice have also shown to induce white adipose tissue browning (Ma et al., 2024). We, thus,

hypothesize that the suppressed hepatocyte expressed CDF is one of the factors playing a role in the mechanisms by which LiB12cKO mice are protected against weigh gain on HFD.

7 Summary/Conclusions

This PhD thesis integrates two primary themes: the application of developed image analysis workflows and the biological investigation of HSD17B12 function in hepatic lipid metabolism. The emphasis was placed on understanding the molecular and cellular mechanisms underlying MASLD and MASH progression, and on establishing robust workflows for their quantitative assessment in preclinical models. A deep learning-based image analysis model was successfully developed to quantify liver steatosis in histological whole-slide images. The integration of this approach with conventional computational histology, electron microscopy, and *in vivo* micro-ultrasound enabled a comprehensive assessment of liver morphology and function.

The hepatocyte-specific knockout of HSD17B12 (LiB12cKO) revealed a distinct phenotype characterized by hepatic lipid accumulation, microvesicular steatosis, hepatocyte hypertrophy, and liver injury. Notably, these mice exhibited resistance to high-fat diet–induced obesity and hepatic steatosis. Transcriptomic analyses supported these findings, indicating altered lipid metabolism and gene expression profiles in LiB12cKO mice. These results suggest that HSD17B12 plays a critical role in lipid droplet expansion and hepatic lipid handling, and its inactivation may offer a novel therapeutic strategy for combating diet-induced obesity and liver disease.

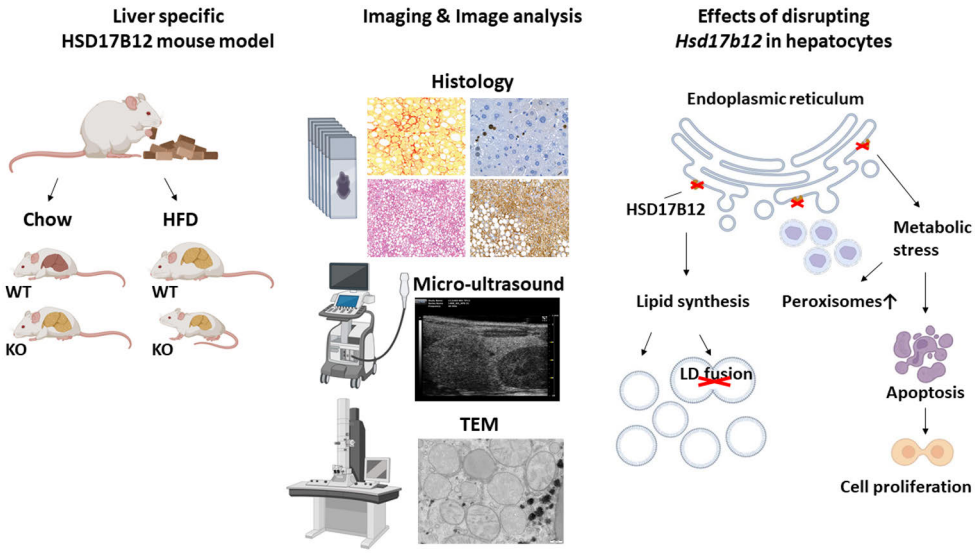

Figure 10. Summary of the research theme of this PhD thesis. Created partly with BioRender.com.

Acknowledgements

This thesis work was carried out at the research Centre for Integrative Physiology and pharmacology (IPP), institute of Biomedicine, University of Turku, Finland during 2020–2025.

I would like to express my deepest gratitude to my supervisors, Professor Matti Poutanen, Docent Leena Strauss, and Adjunct Professor Pekka Ruusuvuori, for the guidance, encouragement, and advice throughout this journey. I have been truly fortunate to have you all as my supervisors. Your feedback has shaped my scientific thinking in countless ways. Matti, you have challenged me to think bigger, see broader connections and maintain a critical perspective. Pekka, you have always been supportive and positive; even though not all projects ended up in this thesis, we shared exciting and innovative work in research and education that fostered creative thinking and the belief that almost anything is possible. Digital pathology is, indeed, fun and cool. Leena, you have been a constant source of support, and I truly believe that without you, I could not have navigated the academic world. Your patience and human-centered approach guided me through challenges, and your expertise and passion for research and teaching have been an inspiration. I also thank my follow-up committee member, Associate Professor Riku Klén, for his guidance and support alongside my supervisors.

I am grateful to the reviewers of this thesis, Professor Alex Odermatt and Docent Veli-Pekka Ronkainen, for their time, valuable comments, and contributions, and to Associate Professor Panu Luukkonen for agreeing to act as my opponent in the public examination.

My sincere thanks go to all research collaborators and co-authors, Hanna Heikelä, David Ekwe, Oluwafemi Ojo, Krisztina Kukoricza, Simone de Brot, Eeva-Liisa Eskelinen, Suvi Ruohonen, Kalle Rytkönen, Asta Laiho, Satu Koskinen, Tomi Suomi, Laura Elo, Sami Blom, Darshan Kumar, Anna Knuuttila, Sonja Boyd, Nelli Sjöblom, Eva-Maria Birkman and many others who contributed to this work.

My special thanks go to the past and present members of the Endocrine Signaling Consortium. Thank you, Hanna Heikelä, for sharing the LiB12cKO mouse project with me. I've learned so much from you about *in vivo* work and practical research, and I'm truly grateful for your guidance. I am grateful to Krisztina Kukoricza,

Guillermo Martinez Nieto, Michael Gabriel, Arttu Junnila, and Julia Mathlin for all the scientific and non-scientific conversations, the invaluable help, and the peer support throughout these years.

The training provided by the Drug Research Doctoral Programme (DRDP, now the Doctoral Programme in Drug Research and Diagnostics (DRD)) has been excellent, and I would like to thank both past and present directors and coordinators of the programme: Ullamari Pesonen, Matti Poutanen, Eeva Valve and Marja Peura. Many thanks to Anni Halonen for her assistance in the final stages of the thesis process.

This work would not have been possible without the support of all past and present professors, principal investigators, researchers, students and technicians in the Department of Physiology: Jorma Toppari, Petra Sipilä, Noora Kotaja, Nafis Rahman, Helena Virtanen, Juho-Antti Mäkelä, Johanna Järvi, Jenni Airaksinen, Pauliina Toivonen, Tanja Kirjonen, Nina Messner, Kamila Pulawska, Konrad Patyra, Opeyemi Olotu, Ammar Ahmenadi, Anna Eggert, Samuli Laasanen, Clara-Theresia Kolehmainen, Katri Hovirinta, Ida Hyötyläinen, Marko Tirri, Tiina Lehtiniemi, Heidi Elamo, Sheila Cisneros Montalvo, Oana Grigoas, Tuula Hämäläinen, Minna Lindroth, Keshav Thapa, Inka Raimoranta and many others.

I was fortunate to supervise the practical work of two excellent master's students. Thank you, Heini Hautanen and David Ekwe, for your valuable contributions to our research!

I would like to thank all the personnel of the Central Animal Laboratory, and *in vivo* experts in TCDM for the good care and help with animal work. Thank you Varpu Laine for helping with the ultrasound imaging. I thank Markus Peurla for his support with the slide scanners and related software and everyone at Histocore for their contributions. Further I thank Markus and Jenni Laine for their assistance with electron microscopy.

My gratitude goes to the "image data goddesses," Joanna and Elnaz. We share the experience of navigating the crosscurrents of doctoral research related to image analysis, academia, working life, and motherhood. Your support as friends means the world to me. Joanna, your help with the thesis figures and the cover image was invaluable, thank you!

I want to thank my mother, Sirkka, and her spouse Anssi, for their support throughout my life. This thesis is dedicated to my mother, who passed away recently. Her lessons are reflected in the way I think, act, and live every single day. To my sister Maija, my brother Pekka, Pete, and Pauliina - thank you for always being there for me. Special thanks for your help in organizing the drinks for the karonkka celebration.

I would also like to acknowledge all my friends for their encouragement and understanding during this long journey: Suvi, Elisa, Mira, Mari, Päivi, Katri, Jenni,

Emmi, and all my other friend – thank you! I am deeply thankful to Eija and Pentti for taking care of Aarni when I needed extra time to write this thesis, and Laura-Maria for her encouragement.

Finally, I want to thank my spouse, Marko. You are my safe rock, and you have always encouraged me to follow my interests and dreams. Thank you for your love and support. And to our dear son, Aarni, I want to say that even though "PhD" is a wonderful title, the most important title for me is being your mom.

This PhD research was financially supported by the Finnish Cultural Foundation, Jalmari and Rauha Ahokas Foundation, Orion research foundation, the Turku University Foundation, The Diabetes Research Foundation, Drug Research Doctoral Programme at the University of Turku and The Medical Faculty of the University of Turku.

27.11.2025

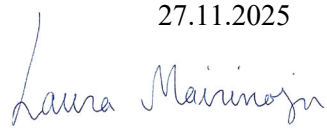

Laura Mairinoja

References

Abdul Jawad, M., & Khursheed, F. (2024). A novel approach for color-balanced reference image selection for breast histology image normalization. *Biomedical Signal Processing and Control*, *94*, 106299. https://doi.org/10.1016/j.bspc.2024.106299

Abul-Husn, N. S., Cheng, X., Li, A. H., Xin, Y., Schurmann, C., Stevis, P., Liu, Y., Kozlitina, J., Stender, S., Wood, G. C., Stepanchick, A. N., Still, M. D., McCarthy, S., O'Dushlaine, C., Packer, J. S., Balasubramanian, S., Gosalia, N., Esopi, D., Kim, S. Y., … Dewey, F. E. (2018). A Protein-Truncating *HSD17B13* Variant and Protection from Chronic Liver Disease. *New England Journal of Medicine*, *378*(12), 1096–1106. https://doi.org/10.1056/NEJMoa1712191

Adam, M., Heikelä, H., Sobolewski, C., Portius, D., Mäki-Jouppila, J., Mehmood, A., Adhikari, P., Esposito, I., Elo, L. L., Zhang, F. P., Ruohonen, S. T., Strauss, L., Foti, M., & Poutanen, M. (2018). Hydroxysteroid (17β) dehydrogenase 13 deficiency triggers hepatic steatosis and inflammation in mice. *FASEB Journal : Official Publication of the Federation of American Societies for Experimental Biology*, *32*(6), 3434–3447. https://doi.org/10.1096/fj.201700914R

Aeffner, F., Adissu, H. A., Boyle, M. C., Cardiff, R. D., Hagendorn, E., Hoenerhoff, M. J., Klopfleisch, R., Newbigging, S., Schaudien, D., Turner, O., & Wilson, K. (2018). Digital Microscopy, Image Analysis, and Virtual Slide Repository. *ILAR Journal*, *59*(1), 66–79. https://doi.org/10.1093/ilar/ily007

Ahmed, A. A., Abouzid, M., & Kaczmarek, E. (2022). Deep Learning Approaches in Histopathology. *Cancers*, *14*(21), 5264. https://doi.org/10.3390/cancers14215264

Ahmed, F., Sellergren, A., Yang, L., Xu, S., Babenko, B., Ward, A., Olson, N., Mohtashamian, A., Matias, Y., Corrado, G. S., Duong, Q., Webster, D. R., Shetty, S., Golden, D., Liu, Y., Steiner, D. F., & Wulczyn, E. (2024). *PathAlign: A vision-language model for whole slide images in histopathology* (Version 1). arXiv. https://doi.org/10.48550/ARXIV.2406.19578

Alamri, Z. Z. (2018). The role of liver in metabolism: An updated review with physiological emphasis. *International Journal of Basic & Clinical Pharmacology*, *7*(11), 2271. https://doi.org/10.18203/2319-2003.ijbcp20184211

Alzubaidi, L., Zhang, J., Humaidi, A. J., Al-Dujaili, A., Duan, Y., Al-Shamma, O., Santamaría, J., Fadhel, M. A., Al-Amidie, M., & Farhan, L. (2021). Review of deep learning: Concepts, CNN architectures, challenges, applications, future directions. *Journal of Big Data*, *8*(1), 53. https://doi.org/10.1186/s40537-021-00444-8

Ayache, J., Beaunier, L., Boumendil, J., Ehret, G., & Laub, D. (2010). Conclusion: What Is a Good Sample? In J. Ayache, L. Beaunier, J. Boumendil, G. Ehret, & D. Laub, *Sample Preparation Handbook for Transmission Electron Microscopy* (pp. 235–236). Springer New York. https://doi.org/10.1007/978-0-387-98182-6_9

Baek, E. B., Lee, J., Hwang, J.-H., Park, H., Lee, B.-S., Kim, Y.-B., Jun, S.-Y., Her, J., Son, H.-Y., & Cho, J.-W. (2023). Application of multiple-finding segmentation utilizing Mask R-CNN-based deep learning in a rat model of drug-induced liver injury. *Scientific Reports*, *13*(1), 17555. https://doi.org/10.1038/s41598-023-44897-8

Bahmanyar, S., & Schlieker, C. (2020). Lipid and protein dynamics that shape nuclear envelope identity. *Molecular Biology of the Cell*, *31*(13), 1315–1323. https://doi.org/10.1091/mbc.E18-10-0636

Bancroft, J. D., & Layton, C. (2019). The hematoxylins and eosin. In *Bancroft's Theory and Practice of Histological Techniques* (pp. 126–138). Elsevier. https://doi.org/10.1016/B978-0-7020-6864-5.00010-4

Banerji, S., & Mitra, S. (2022). Deep learning in histopathology: A review. *WIREs Data Mining and Knowledge Discovery*, *12*(1), e1439. https://doi.org/10.1002/widm.1439

Bankhead, P. (2025). Files & file formats. In *Introduction to Bioimage Analysis*. https://bioimagebook.github.io/

Bankhead, P., Loughrey, M. B., Fernández, J. A., Dombrowski, Y., McArt, D. G., Dunne, P. D., McQuaid, S., Gray, R. T., Murray, L. J., Coleman, H. G., James, J. A., Salto-Tellez, M., & Hamilton, P. W. (2017). QuPath: Open source software for digital pathology image analysis. *Scientific Reports*, *7*(1), 16878. https://doi.org/10.1038/s41598-017-17204-5

Banning, A., Deubel, S., Kluth, D., Zhou, Z., & Brigelius-Flohé, R. (2005). The GI-GPx gene is a target for Nrf2. *GBM Annual Fall Meeting Berlin/Potsdam 2005*, *2005*(Fall), 1282. https://doi.org/10.1240/sav_gbm_2005_h_001282

Betyna, M., & Zieliński, E. (2018). *Histology – History, Short Review Of Techniques And Application In Modern Science*. https://doi.org/10.5281/ZENODO.1442533

Breitling, R., Marijanović, Z., Perović, D., & Adamski, J. (2001). Evolution of 17β-HSD type 4, a multifunctional protein of β-oxidation. *Molecular and Cellular Endocrinology*, *171*(1–2), 205–210. https://doi.org/10.1016/S0303-7207(00)00415-9

Brixtel, R., Bougleux, S., Lezoray, O., Caillot, Y., Lemoine, B., Fontaine, M., Nebati, D., & Renouf, A. (2022). Whole Slide Image Quality in Digital Pathology: Review and Perspectives. *IEEE Access*, *10*, 131005–131035. https://doi.org/10.1109/ACCESS.2022.3227437

Chalasani, N., Younossi, Z., Lavine, J. E., Charlton, M., Cusi, K., Rinella, M., Harrison, S. A., Brunt, E. M., & Sanyal, A. J. (2018). The diagnosis and management of nonalcoholic fatty liver disease: Practice guidance from the American Association for the Study of Liver Diseases. *Hepatology (Baltimore, Md.)*, *67*(1), 328–357. https://doi.org/10.1002/hep.29367

Chen, R., Liu, Y., Kong, L., Chen, N., Zhu, X., Ma, Y., Liu, T., & Wang, W. (2023). *Towards Label-free Scene Understanding by Vision Foundation Models* (Version 2). arXiv. https://doi.org/10.48550/ARXIV.2306.03899

Clark, I., & Torbenson, M. S. (2017). Immunohistochemistry and Special Stains in Medical Liver Pathology. *Advances in Anatomic Pathology*, *24*(2), 99–109. https://doi.org/10.1097/PAP.0000000000000139

Clunie, D. A. (2021). DICOM Format and Protocol Standardization—A Core Requirement for Digital Pathology Success. *Toxicologic Pathology*, *49*(4), 738–749. https://doi.org/10.1177/0192623320965893

Colemonts-Vroninks, H., Neuckermans, J., Marcelis, L., Claes, P., Branson, S., Casimir, G., Goyens, P., Martens, G. A., Vanhaecke, T., & De Kock, J. (2020). Oxidative Stress, Glutathione Metabolism, and Liver Regeneration Pathways Are Activated in Hereditary Tyrosinemia Type 1 Mice upon Short-Term Nitisinone Discontinuation. *Genes*, *12*(1), 3. https://doi.org/10.3390/genes12010003

Cooper, M., Ji, Z., & Krishnan, R. G. (2023). Machine learning in computational histopathology: Challenges and opportunities. *Genes, Chromosomes and Cancer*, *62*(9), 540–556. https://doi.org/10.1002/gcc.23177

Cootney, R. W. (2001). Ultrasound Imaging: Principles and Applications in Rodent Research. *ILAR Journal*, *42*(3), 233–247. https://doi.org/10.1093/ilar.42.3.233

Crane, J. D., Barrandon, O., Faherty, B., Gorgoglione, M., Crowley, C., Morin, J., Ross, T. T., Shimkonis, J., Li, D., Hirenallur-Shanthappa, D., Boucher, M., Ahn, Y., & Clasquin, M. F. (2024). Murine HSD17β13 does not control liver steatosis and modestly impacts fibrosis in a sex- and diet-

specific manner. *Journal of Lipid Research*, *65*(10), 100634. https://doi.org/10.1016/j.jlr.2024.100634

Dahan, C., Christodoulidis, S., Vakalopoulou, M., & Boyd, J. (2022). *Artifact Removal in Histopathology Images* (Version 2). arXiv. https://doi.org/10.48550/ARXIV.2211.16161

Dana, J., Venkatasamy, A., Saviano, A., Lupberger, J., Hoshida, Y., Vilgrain, V., Nahon, P., Reinhold, C., Gallix, B., & Baumert, T. F. (2022). Conventional and artificial intelligence-based imaging for biomarker discovery in chronic liver disease. *Hepatology International*, *16*(3), 509–522. https://doi.org/10.1007/s12072-022-10303-0

Desai, C., Lohani, S., Sharma, A. R., Schwartz, L., Gujjula, S. R., Baskar, A., Baskar, U., Baskar, S., & Vasikaran, A. (2025). Lean Metabolic Dysfunction-Associated Steatotic Liver Disease: A Comparative Analysis of Hepatic and Oncological Outcomes. *Journal of Clinical Gastroenterology*. https://doi.org/10.1097/MCG.0000000000002153

Di Lascio, N., Kusmic, C., Stea, F., Lenzarini, F., Barsanti, C., Leloup, A., & Faita, F. (2018). Longitudinal micro-ultrasound assessment of the ob/ob mouse model: Evaluation of cardiovascular, renal and hepatic parameters. *International Journal of Obesity*, *42*(3), 518–524. https://doi.org/10.1038/ijo.2017.219

Dimitriou, N., Arandjelović, O., & Caie, P. D. (2019). Deep Learning for Whole Slide Image Analysis: An Overview. *Frontiers in Medicine*, *6*, 264. https://doi.org/10.3389/fmed.2019.00264

Dornbush, S., & Aeddula, N. R. (2025). Physiology, Leptin. In *StatPearls*. StatPearls Publishing. http://www.ncbi.nlm.nih.gov/books/NBK537038/

Evans, T., Retzlaff, C. O., Geißler, C., Kargl, M., Plass, M., Müller, H., Kiehl, T.-R., Zerbe, N., & Holzinger, A. (2022). The explainability paradox: Challenges for xAI in digital pathology. *Future Generation Computer Systems*, *133*, 281–296. https://doi.org/10.1016/j.future.2022.03.009

Faita, F., Di Lascio, N., Rossi, C., Kusmic, C., & Solini, A. (2018). Ultrasonographic Characterization of the *db/db* Mouse: An Animal Model of Metabolic Abnormalities. *Journal of Diabetes Research*, *2018*, 1–9. https://doi.org/10.1155/2018/4561309

Fang, T., Wang, H., Pan, X., Little, P. J., Xu, S., & Weng, J. (2022). Mouse models of nonalcoholic fatty liver disease (NAFLD): Pathomechanisms and pharmacotherapies. *International Journal of Biological Sciences*, *18*(15), 5681–5697. https://doi.org/10.7150/ijbs.65044

Farooqi, I. S., & Xu, Y. (2024). Translational potential of mouse models of human metabolic disease. *Cell*, *187*(16), 4129–4143. https://doi.org/10.1016/j.cell.2024.07.011

Farrell, G., Schattenberg, J. M., Leclercq, I., Yeh, M. M., Goldin, R., Teoh, N., & Schuppan, D. (2019). Mouse Models of Nonalcoholic Steatohepatitis: Toward Optimization of Their Relevance to Human Nonalcoholic Steatohepatitis. *Hepatology*, *69*(5), 2241–2257. https://doi.org/10.1002/hep.30333

Feldman, A. T., & Wolfe, D. (2014). Tissue Processing and Hematoxylin and Eosin Staining. In C. E. Day (Ed.), *Histopathology* (Vol. 1180, pp. 31–43). Springer New York. https://doi.org/10.1007/978-1-4939-1050-2_3

Ferdinandusse, S., & Houten, S. M. (2006). Peroxisomes and bile acid biosynthesis. *Biochimica et Biophysica Acta (BBA) - Molecular Cell Research*, *1763*(12), 1427–1440. https://doi.org/10.1016/j.bbamcr.2006.09.001

Fitzpatrick, E. (2014). Noninvasive biomarkers in non-alcoholic fatty liver disease: Current status and a glimpse of the future. *World Journal of Gastroenterology*, *20*(31), 10851. https://doi.org/10.3748/wjg.v20.i31.10851

Flessa, C.-M., Nasiri-Ansari, N., Kyrou, I., Leca, B. M., Lianou, M., Chatzigeorgiou, A., Kaltsas, G., Kassi, E., & Randeva, H. S. (2022). Genetic and Diet-Induced Animal Models for Non-Alcoholic Fatty Liver Disease (NAFLD) Research. *International Journal of Molecular Sciences*, *23*(24), 15791. https://doi.org/10.3390/ijms232415791

Foster, F. S., Pavlin, C. J., Harasiewicz, K. A., Christopher, D. A., & Turnbull, D. H. (2000). Advances in ultrasound biomicroscopy. *Ultrasound in Medicine & Biology*, *26*(1), 1–27. https://doi.org/10.1016/S0301-5629(99)00096-4

Gadi, Z., Kwanten, W. J., Vonghia, L., & Francque, S. M. (2024). MASH to cirrhosis: Bridging the gaps in MASLD management. *Acta Clinica Belgica*, *79*(6), 441–450. https://doi.org/10.1080/17843286.2025.2466011

Gautam, J., Aggarwal, H., Kumari, D., Gupta, S. K., Kumar, Y., & Dikshit, M. (2024). A methionine-choline-deficient diet induces nonalcoholic steatohepatitis and alters the lipidome, metabolome, and gut microbiome profile in the C57BL/6J mouse. *Biochimica et Biophysica Acta (BBA) - Molecular and Cell Biology of Lipids*, *1869*(8), 159545. https://doi.org/10.1016/j.bbalip.2024.159545

Ge, F., Lobdell, H., Zhou, S., Hu, C., & Berk, P. D. (2010). Digital analysis of hepatic sections in mice accurately quantitates triglycerides and selected properties of lipid droplets. *Experimental Biology and Medicine*, *235*(11), 1282–1286. https://doi.org/10.1258/ebm.2010.010095

Gofton, C., Upendran, Y., Zheng, M.-H., & George, J. (2023). MAFLD: How is it different from NAFLD? *Clinical and Molecular Hepatology*, *29*(Suppl), S17–S31. https://doi.org/10.3350/cmh.2022.0367

Grignaffini, F., Barbuto, F., Troiano, M., Piazzo, L., Simeoni, P., Mangini, F., De Stefanis, C., Onetti Muda, A., Frezza, F., & Alisi, A. (2024). The Use of Artificial Intelligence in the Liver Histopathology Field: A Systematic Review. *Diagnostics*, *14*(4), 388. https://doi.org/10.3390/diagnostics14040388

Guo, X., Wang, F., Teodoro, G., Farris, A. B., & Kong, J. (2019). Liver Steatosis Segmentation With Deep Learning Methods. *2019 IEEE 16th International Symposium on Biomedical Imaging (ISBI 2019)*, 24–27. https://doi.org/10.1109/ISBI.2019.8759600

Guy, C. D., Suzuki, A., Burchette, J. L., Brunt, E. M., Abdelmalek, M. F., Cardona, D., McCall, S. J., Ünalp, A., Belt, P., Ferrell, L. D., & Diehl, A. M. (2012). Costaining for keratins 8/18 plus ubiquitin improves detection of hepatocyte injury in nonalcoholic fatty liver disease. *Human Pathology*, *43*(6), 790–800. https://doi.org/10.1016/j.humpath.2011.07.007

Haase, R., Fazeli, E., Legland, D., Doube, M., Culley, S., Belevich, I., Jokitalo, E., Schorb, M., Klemm, A., & Tischer, C. (2022). A Hitchhiker's guide through the bio-image analysis software universe. *FEBS Letters*, *596*(19), 2472–2485. https://doi.org/10.1002/1873-3468.14451

Hachim, M. Y., Aljaibeji, H., Hamoudi, R. A., Hachim, I. Y., Elemam, N. M., Mohammed, A. K., Salehi, A., Taneera, J., & Sulaiman, N. (2020). An Integrative Phenotype–Genotype Approach Using Phenotypic Characteristics from the UAE National Diabetes Study Identifies HSD17B12 as a Candidate Gene for Obesity and Type 2 Diabetes. *Genes*, *11*(4), 461. https://doi.org/10.3390/genes11040461

Hansen, H. H., Feigh, M., Veidal, S. S., Rigbolt, K. T., Vrang, N., & Fosgerau, K. (2017). Mouse models of nonalcoholic steatohepatitis in preclinical drug development. *Drug Discovery Today*, *22*(11), 1707–1718. https://doi.org/10.1016/j.drudis.2017.06.007

Harris, S. E., Poolman, T. M., Arvaniti, A., Cox, R. D., Gathercole, L. L., & Tomlinson, J. W. (2020). The American lifestyle-induced obesity syndrome diet in male and female rodents recapitulates the clinical and transcriptomic features of nonalcoholic fatty liver disease and nonalcoholic steatohepatitis. *American Journal of Physiology-Gastrointestinal and Liver Physiology*, *319*(3), G345–G360. https://doi.org/10.1152/ajpgi.00055.2020

Havranek, B., Loh, R., Torre, B., Redfield, R., & Halegoua-DeMarzio, D. (2025). Glucagon-like peptide-1 receptor agonists improve metabolic dysfunction-associated steatotic liver disease outcomes. *Scientific Reports*, *15*(1). https://doi.org/10.1038/s41598-025-89408-z

Heeren, J., & Scheja, L. (2021). Metabolic-associated fatty liver disease and lipoprotein metabolism. *Molecular Metabolism*, *50*, 101238. https://doi.org/10.1016/j.molmet.2021.101238

Heikelä, H., Mairinoja, L., Ruohonen, S. T., Rytkönen, K. T., De Brot, S., Laiho, A., Koskinen, S., Suomi, T., Elo, L. L., Strauss, L., & Poutanen, M. (2024). Disruption of HSD17B12 in mouse hepatocytes leads to reduced body weight and defect in the lipid droplet expansion associated with microvesicular steatosis. *The FASEB Journal*, *38*(17), e70034. https://doi.org/10.1096/fj.202400333RR

Heikelä, H., Ruohonen, S. T., Adam, M., Viitanen, R., Liljenbäck, H., Eskola, O., Gabriel, M., Mairinoja, L., Pessia, A., Velagapudi, V., Roivainen, A., Zhang, F. P., Strauss, L., & Poutanen, M. (2020). Hydroxysteroid (17β) dehydrogenase 12 is essential for metabolic homeostasis in adult

mice. *American Journal of Physiology.Endocrinology and Metabolism*, *319*(3), E494–E508. https://doi.org/10.1152/ajpendo.00042.2020

Heinemann, F., Birk, G., & Stierstorfer, B. (2019). Deep learning enables pathologist-like scoring of NASH models. *Scientific Reports*, *9*(1), 18454. https://doi.org/10.1038/s41598-019-54904-6

Hofmann, K., Tomiuk, S., Wolff, G., & Stoffel, W. (2000). Cloning and characterization of the mammalian brain-specific, Mg $^{2+}$ -dependent neutral sphingomyelinase. *Proceedings of the National Academy of Sciences*, *97*(11), 5895–5900. https://doi.org/10.1073/pnas.97.11.5895

Horiguchi, Y., Araki, M., & Motojima, K. (2008a). 17β-Hydroxysteroid dehydrogenase type 13 is a liver-specific lipid droplet-associated protein. *Biochemical and Biophysical Research Communications*, *370*(2), 235–238. https://doi.org/10.1016/j.bbrc.2008.03.063

Horiguchi, Y., Araki, M., & Motojima, K. (2008b). Identification and characterization of the ER/lipid droplet-targeting sequence in 17β-hydroxysteroid dehydrogenase type 11. *Archives of Biochemistry and Biophysics*, *479*(2), 121–130. https://doi.org/10.1016/j.abb.2008.08.020

Huang, D. W., Sherman, B. T., & Lempicki, R. A. (2009). Systematic and integrative analysis of large gene lists using DAVID bioinformatics resources. *Nature Protocols*, *4*(1), 44–57. https://doi.org/10.1038/nprot.2008.211

Hwang, J.-H., Lim, M., Han, G., Park, H., Kim, Y.-B., Park, J., Jun, S.-Y., Lee, J., & Cho, J.-W. (2023). Segmentation algorithm can be used for detecting hepatic fibrosis in SD rat. *Laboratory Animal Research*, *39*(1), 16. https://doi.org/10.1186/s42826-023-00167-2

Inoue, T., & Yagi, Y. (2020). Color standardization and optimization in whole slide imaging. *Clinical and Diagnostic Pathology*, *4*(1). https://doi.org/10.15761/cdp.1000139

Irshad, H., Veillard, A., Roux, L., & Racoceanu, D. (2014). Methods for Nuclei Detection, Segmentation, and Classification in Digital Histopathology: A Review—Current Status and Future Potential. *IEEE Reviews in Biomedical Engineering*, *7*, 97–114. https://doi.org/10.1109/RBME.2013.2295804

Jaeschke, H. (2002). Mechanisms of Hepatotoxicity. *Toxicological Sciences*, *65*(2), 166–176. https://doi.org/10.1093/toxsci/65.2.166

Jensen, E. L., Israelsen, M., & Krag, A. (2024). Transforming steatotic liver disease management: The emerging role of GLP-1 receptor agonists. *Hepatology Communications*, *8*(11). https://doi.org/10.1097/hc9.0000000000000561

Jeong, B.-K., Choi, W.-I., Choi, W., Moon, J., Lee, W. H., Choi, C., Choi, I. Y., Lee, S.-H., Kim, J. K., Ju, Y. S., Kim, P., Moon, Y.-A., Park, J. Y., & Kim, H. (2024). A male mouse model for metabolic dysfunction-associated steatotic liver disease and hepatocellular carcinoma. *Nature Communications*, *15*(1), 6506. https://doi.org/10.1038/s41467-024-50660-y

Jokela, H., Rantakari, P., Lamminen, T., Strauss, L., Ola, R., Mutka, A.-L., Gylling, H., Miettinen, T., Pakarinen, P., Sainio, K., & Poutanen, M. (2010). Hydroxysteroid (17β) Dehydrogenase 7 Activity Is Essential for Fetal de Novo Cholesterol Synthesis and for Neuroectodermal Survival and Cardiovascular Differentiation in Early Mouse Embryos. *Endocrinology*, *151*(4), 1884–1892. https://doi.org/10.1210/en.2009-0928

Kaiser, D., Inciuraite, G., & Cichy, R. M. (2020). Rapid contextualization of fragmented scene information in the human visual system. *NeuroImage*, *219*, 117045. https://doi.org/10.1016/j.neuroimage.2020.117045

Karagoz, M. A., Akay, B., Basturk, A., Karaboga, D., & Nalbantoglu, O. U. (2023). An unsupervised transfer learning model based on convolutional auto encoder for non-alcoholic steatohepatitis activity scoring and fibrosis staging of liver histopathological images. *Neural Computing and Applications*, *35*(14), 10605–10619. https://doi.org/10.1007/s00521-023-08252-2

Kartasalo, K., Latonen, L., Vihinen, J., Visakorpi, T., Nykter, M., & Ruusuvuori, P. (2018). Comparative analysis of tissue reconstruction algorithms for 3D histology. *Bioinformatics (Oxford, England)*, *34*(17), 3013–3021. https://doi.org/10.1093/bioinformatics/bty210

Ke, J., Liu, K., Sun, Y., Xue, Y., Huang, J., Lu, Y., Dai, J., Chen, Y., Han, X., Shen, Y., & Shen, D. (2023). Artifact Detection and Restoration in Histology Images With Stain-Style and Structural

Preservation. *IEEE Transactions on Medical Imaging*, *42*(12), 3487–3500. https://doi.org/10.1109/TMI.2023.3288940

Kemiläinen, H., Adam, M., Mäki-Jouppila, J., Damdimopoulou, P., Damdimopoulos, A. E., Kere, J., Hovatta, O., Laajala, T. D., Aittokallio, T., Adamski, J., Ryberg, H., Ohlsson, C., Strauss, L., & Poutanen, M. (2016). The Hydroxysteroid (17β) Dehydrogenase Family Gene HSD17B12 Is Involved in the Prostaglandin Synthesis Pathway, the Ovarian Function, and Regulation of Fertility. *Endocrinology*, *157*(10), 3719–3730. https://doi.org/10.1210/en.2016-1252

Khan, U., Härkönen, J., Friman, M., Latonen, L., Kuopio, T., & Ruusuvuori, P. (2025). *Staining normalization in histopathology: Method benchmarking using multicenter dataset* (Version 1). arXiv. https://doi.org/10.48550/ARXIV.2506.19106

Khan, U., Koivukoski, S., Valkonen, M., Latonen, L., & Ruusuvuori, P. (2023). The effect of neural network architecture on virtual H&E staining: Systematic assessment of histological feasibility. *Patterns*, *4*(5), 100725. https://doi.org/10.1016/j.patter.2023.100725

Kim, H.-J., Baek, E. B., Hwang, J.-H., Lim, M., Jung, W. H., Bae, M. A., Son, H.-Y., & Cho, J.-W. (2023). Application of convolutional neural network for analyzing hepatic fibrosis in mice. *Journal of Toxicologic Pathology*, *36*(1), 21–30. https://doi.org/10.1293/tox.2022-0066

Kim, S.-W., Roh, J., & Park, C.-S. (2016). Immunohistochemistry for Pathologists: Protocols, Pitfalls, and Tips. *Journal of Pathology and Translational Medicine*, *50*(6), 411–418. https://doi.org/10.4132/jptm.2016.08.08

Kleiner, D. E., Brunt, E. M., Van Natta, M., Behling, C., Contos, M. J., Cummings, O. W., Ferrell, L. D., Liu, Y.-C., Torbenson, M. S., Unalp-Arida, A., Yeh, M., McCullough, A. J., Sanyal, A. J., & Nonalcoholic Steatohepatitis Clinical Research Network. (2005). Design and validation of a histological scoring system for nonalcoholic fatty liver disease. *Hepatology*, *41*(6), 1313–1321. https://doi.org/10.1002/hep.20701

Kleiner, D. E., Chalasani, N. P., Lee, W. M., Fontana, R. J., Bonkovsky, H. L., Watkins, P. B., Hayashi, P. H., Davern, T. J., Navarro, V., Reddy, R., Talwalkar, J. A., Stolz, A., Gu, J., Barnhart, H., Hoofnagle, J. H., & Drug-Induced Liver Injury Network (DILIN). (2014). Hepatic histological findings in suspected drug-induced liver injury: Systematic evaluation and clinical associations. *Hepatology (Baltimore, Md.)*, *59*(2), 661–670. PubMed. https://doi.org/10.1002/hep.26709

Koivukoski, S., Khan, U., Ruusuvuori, P., & Latonen, L. (2023). Unstained Tissue Imaging and Virtual Hematoxylin and Eosin Staining of Histologic Whole Slide Images. *Laboratory Investigation*, *103*(5), 100070. https://doi.org/10.1016/j.labinv.2023.100070

Kotian, T. (2024). Computational pathology—Transforming diagnosis through machine learning and AI. *IP Journal of Diagnostic Pathology and Oncology*, *9*(3), 146–150. https://doi.org/10.18231/j.jdpo.2024.030

Kristiani, L., & Kim, Y. (2023). The Interplay between Oxidative Stress and the Nuclear Lamina Contributes to Laminopathies and Age-Related Diseases. *Cells*, *12*(9), 1234. https://doi.org/10.3390/cells12091234

Kruepunga, N., Hakvoort, T. B. M., Hikspoors, J. P. J. M., Köhler, S. E., & Lamers, W. H. (2019). Anatomy of rodent and human livers: What are the differences? *Biochimica et Biophysica Acta (BBA) - Molecular Basis of Disease*, *1865*(5), 869–878. https://doi.org/10.1016/j.bbadis.2018.05.019

Kulyté, A., Aman, A., Strawbridge, R. J., Arner, P., & Dahlman, I. A. (2022). Genome-Wide Association Study Identifies Genetic Loci Associated With Fat Cell Number and Overlap With Genetic Risk Loci for Type 2 Diabetes. *Diabetes*, *71*(6), 1350–1362. https://doi.org/10.2337/db21-0804

Laajala, T. D., Jumppanen, M., Huhtaniemi, R., Fey, V., Kaur, A., Knuuttila, M., Aho, E., Oksala, R., Westermarck, J., Mäkelä, S., Poutanen, M., & Aittokallio, T. (2016). Optimized design and analysis of preclinical intervention studies in vivo. *Scientific Reports*, *6*(1), 30723. https://doi.org/10.1038/srep30723

Latonen, L., Koivukoski, S., Khan, U., & Ruusuvuori, P. (2024). Virtual staining for histology by deep learning. *Trends in Biotechnology*, *42*(9), 1177–1191. https://doi.org/10.1016/j.tibtech.2024.02.009

Laurino, A., Franceschini, A., Pesce, L., Cinci, L., Montalbano, A., Mazzamuto, G., Sancataldo, G., Nesi, G., Costantini, I., Silvestri, L., & Pavone, F. S. (2023). A Guide to Perform 3D Histology of Biological Tissues with Fluorescence Microscopy. *International Journal of Molecular Sciences*, *24*(7), 6747. https://doi.org/10.3390/ijms24076747

LeCun, Y., Bengio, Y., & Hinton, G. (2015). Deep learning. *Nature*, *521*(7553), 436–444. https://doi.org/10.1038/nature14539

Lefkowitch, J. H., Haythe, J. H., & Regent, N. (2002). Kupffer Cell Aggregation and Perivenular Distribution in Steatohepatitis. *Modern Pathology*, *15*(7), 699–704. https://doi.org/10.1097/01.MP.0000019579.30842.96

Lessa, A. S., Paredes, B. D., Dias, J. V., Carvalho, A. B., Quintanilha, L. F., Takiya, C. M., Tura, B. R., Rezende, G. F., Campos De Carvalho, A. C., Resende, C. M., & Goldenberg, R. C. (2010). Ultrasound imaging in an experimental model of fatty liver disease and cirrhosis in rats. *BMC Veterinary Research*, *6*(1), 6. https://doi.org/10.1186/1746-6148-6-6

Levene, A. P., Kudo, H., Armstrong, M. J., Thursz, M. R., Gedroyc, W. M., Anstee, Q. M., & Goldin, R. D. (2012). Quantifying hepatic steatosis – more than meets the eye. *Histopathology*, *60*(6), 971–981. https://doi.org/10.1111/j.1365-2559.2012.04193.x

Li, Y., Zheng, T., Xiao, S., Wang, P., Yang, W., Jiang, L., Chen, L., Sha, J., Jin, Y., Chen, S., Byrne, C. D., Targher, G., Li, J., & Zheng, M. (2023). Hepatocytic ballooning in non-alcoholic steatohepatitis: Dilemmas and future directions. *Liver International*, *43*(6), 1170–1182. https://doi.org/10.1111/liv.15571

Liang, P., Pu, B., Huang, H., Li, Y., Wang, H., Ma, W., & Chang, Q. (2025). *Vision Foundation Models in Medical Image Analysis: Advances and Challenges* (Version 2). arXiv. https://doi.org/10.48550/ARXIV.2502.14584

Liang, W., Menke, A. L., Driessen, A., Koek, G. H., Lindeman, J. H., Stoop, R., Havekes, L. M., Kleemann, R., & van den Hoek, A. M. (2014). Establishment of a General NAFLD Scoring System for Rodent Models and Comparison to Human Liver Pathology. *PLoS ONE*, *9*(12), e115922. https://doi.org/10.1371/journal.pone.0115922

Liu, W., Wang, X., Wang, Y., Wang, Y., Zhang, J., Shi, B., & Li, C. (2021). Three-dimensional reconstruction of systematic histological sections: Application to observations on palatal shelf elevation. *International Journal of Oral Science*, *13*(1), 17. https://doi.org/10.1038/s41368-021-00122-8

Lockwood, G. R., Turnball, D. H., Christopher, D. A., & Foster, F. S. (1996). Beyond 30 MHz [applications of high-frequency ultrasound imaging]. *IEEE Engineering in Medicine and Biology Magazine*, *15*(6), 60–71. https://doi.org/10.1109/51.544513

Lu, F., Zheng, K. I., Rios, R. S., Targher, G., Byrne, C. D., & Zheng, M. (2020). Global epidemiology of lean non-alcoholic fatty liver disease: A systematic review and meta-analysis. *Journal of Gastroenterology and Hepatology*, *35*(12), 2041–2050. https://doi.org/10.1111/jgh.15156

Lukacik, P., Kavanagh, K. L., & Oppermann, U. (2006). Structure and function of human 17β-hydroxysteroid dehydrogenases. *Molecular and Cellular Endocrinology*, *248*(1–2), 61–71. https://doi.org/10.1016/j.mce.2005.12.007

Luukkonen, P. K., Sakuma, I., Gaspar, R. C., Mooring, M., Nasiri, A., Kahn, M., Zhang, X.-M., Zhang, D., Sammalkorpi, H., Penttilä, A. K., Orho-Melander, M., Arola, J., Juuti, A., Zhang, X., Yimlamai, D., Yki-Järvinen, H., Petersen, K. F., & Shulman, G. I. (2023). Inhibition of *HSD17B13* protects against liver fibrosis by inhibition of pyrimidine catabolism in nonalcoholic steatohepatitis. *Proceedings of the National Academy of Sciences*, *120*(4), e2217543120. https://doi.org/10.1073/pnas.2217543120

Luukkonen, P. K., Tukiainen, T., Juuti, A., Sammalkorpi, H., Haridas, P. A. N., Niemelä, O., Arola, J., Orho-Melander, M., Hakkarainen, A., Kovanen, P. T., Dwivedi, O., Groop, L., Hodson, L., Gastaldelli, A., Hyötyläinen, T., Orešič, M., & Yki-Järvinen, H. (2020). Hydroxysteroid 17-β dehydrogenase 13 variant increases phospholipids and protects against fibrosis in nonalcoholic fatty liver disease. *JCI Insight*, *5*(5), e132158. https://doi.org/10.1172/jci.insight.132158

Lyu, X., Wang, J., Wang, J., Yin, Y.-S., Zhu, Y., Li, L.-L., Huang, S., Peng, S., Xue, B., Liao, R., Wang, S.-Q., Long, M., Wohland, T., Chua, B. T., Sun, Y., Li, P., Chen, X.-W., Xu, L., Chen, F.-J., & Li, P. (2021). A gel-like condensation of Cidec generates lipid-permeable plates for lipid droplet fusion. *Developmental Cell*, *56*(18), 2592-2606.e7. https://doi.org/10.1016/j.devcel.2021.08.015

Ma, L., Gilani, A., Rubio-Navarro, A., Cortada, E., Li, A., Reilly, S. M., Tang, L., & Lo, J. C. (2024). Adipsin and adipocyte-derived C3aR1 regulate thermogenic fat in a sex-dependent fashion. *JCI Insight*, *9*(11), e178925. https://doi.org/10.1172/jci.insight.178925

Ma, L., Rathgeb, A., Mubarak, H., Tran, M., & Fei, B. (2022). Unsupervised super-resolution reconstruction of hyperspectral histology images for whole-slide imaging. *Journal of Biomedical Optics*, *27*(05). https://doi.org/10.1117/1.JBO.27.5.056502

Ma, Y., Brown, P. M., Lin, D. D., Ma, J., Feng, D., Belyaeva, O. V., Podszun, M. C., Roszik, J., Allen, J. N., Umarova, R., Kleiner, D. E., Kedishvili, N. Y., Gavrilova, O., Gao, B., & Rotman, Y. (2021). 17-Beta Hydroxysteroid Dehydrogenase 13 Deficiency Does Not Protect Mice From Obesogenic Diet Injury. *Hepatology*, *73*(5), 1701–1716. https://doi.org/10.1002/hep.31517

Mamou, J., & Oelze, M. L. (Eds.). (2013). *Quantitative Ultrasound in Soft Tissues*. Springer Netherlands. https://doi.org/10.1007/978-94-007-6952-6

McNeil, C., Wong, P. F., Sridhar, N., Wang, Y., Santori, C., Wu, C.-H., Homyk, A., Gutierrez, M., Behrooz, A., Tiniakos, D., Burt, A. D., Pai, R. K., Tekiela, K., Patel, H., Cameron Chen, P.-H., Fischer, L., Martins, E. B., Seyedkazemi, S., Freedman, D., … Cimermancic, P. (2024). An End-to-End Platform for Digital Pathology Using Hyperspectral Autofluorescence Microscopy and Deep Learning-Based Virtual Histology. *Modern Pathology*, *37*(2), 100377. https://doi.org/10.1016/j.modpat.2023.100377

Milek, M., Moulla, Y., Kern, M., Stroh, C., Dietrich, A., Schön, M. R., Gärtner, D., Lohmann, T., Dressler, M., Kovacs, P., Stumvoll, M., Blüher, M., & Guiu-Jurado, E. (2022). Adipsin Serum Concentrations and Adipose Tissue Expression in People with Obesity and Type 2 Diabetes. *International Journal of Molecular Sciences*, *23*(4), 2222. https://doi.org/10.3390/ijms23042222

Mohamed, B., Mazeaud, C., Baril, M., Poirier, D., Sow, A. A., Chatel-Chaix, L., Titorenko, V., & Lamarre, D. (2020). Very-long-chain fatty acid metabolic capacity of 17-beta-hydroxysteroid dehydrogenase type 12 (HSD17B12) promotes replication of hepatitis C virus and related flaviviruses. *Scientific Reports*, *10*(1), 4040. https://doi.org/10.1038/s41598-020-61051-w

Moon, Y. A., & Horton, J. D. (2003). Identification of two mammalian reductases involved in the two-carbon fatty acyl elongation cascade. *The Journal of Biological Chemistry*, *278*(9), 7335–7343. https://doi.org/10.1074/jbc.M211684200

Murakami, T., Yasuda, Y., Mita, S., Maeda, S., Shimada, K., Fujimoto, T., & Araki, S. (1987). Prealbumin gene expression during mouse development studied by in situ hybridization. *Cell Differentiation*, *22*(1), 1–9. https://doi.org/10.1016/0045-6039(87)90408-8

Neuman, M. G., Cohen, L. B., & Nanau, R. M. (2014). Biomarkers in Nonalcoholic Fatty Liver Disease. *Canadian Journal of Gastroenterology and Hepatology*, *28*(11), 607–618. https://doi.org/10.1155/2014/757929

Pandit, H., Tinney, J. P., Li, Y., Cui, G., Li, S., Keller, B. B., & Martin, R. C. G. (2019). Utilizing Contrast-Enhanced Ultrasound Imaging for Evaluating Fatty Liver Disease Progression in Pre-clinical Mouse Models. *Ultrasound in Medicine & Biology*, *45*(2), 549–557. https://doi.org/10.1016/j.ultrasmedbio.2018.10.011

Pantanowitz, L., & Parwani, A. V. (2017). *Digital pathology*. American Society for Clinical Pathology Press.

Park, J., Lee, J. M., Lee, G., Jeon, S. K., & Joo, I. (2022). Quantitative Evaluation of Hepatic Steatosis Using Advanced Imaging Techniques: Focusing on New Quantitative Ultrasound Techniques. *Korean Journal of Radiology*, *23*(1), 13. https://doi.org/10.3348/kjr.2021.0112

Parlakgül, G., Pang, S., Artico, L. L., Min, N., Cagampan, E., Villa, R., Goncalves, R. L. S., Lee, G. Y., Xu, C. S., Hotamışlıgil, G. S., & Arruda, A. P. (2024). Spatial mapping of hepatic ER and

mitochondria architecture reveals zonated remodeling in fasting and obesity. *Nature Communications*, *15*(1), 3982. https://doi.org/10.1038/s41467-024-48272-7

Parsons, G. (2023). Understanding liver function tests: Part 1. *Prescriber*, *34*(7), 19–23. https://doi.org/10.1002/psb.2079

Pawlina, W. (2024). Digestive system III: Liver gallbladder and pancreas. In *Histology: A text and atlas: With correlated cell and molecular biology* (Ninth edition, international edition, pp. 692–708). Wolters Kluwer.

Peleman, C., De Vos, W. H., Pintelon, I., Driessen, A., Van Eyck, A., Van Steenkiste, C., Vonghia, L., De Man, J., De Winter, B. Y., Vanden Berghe, T., Francque, S. M., & Kwanten, W. J. (2023). Zonated quantification of immunohistochemistry in normal and steatotic livers. *Virchows Archiv*, *482*(6), 1035–1045. https://doi.org/10.1007/s00428-023-03496-8

Pillar, N., Li, Y., Zhang, Y., & Ozcan, A. (2024). Virtual Staining of Nonfixed Tissue Histology. *Modern Pathology*, *37*(5), 100444. https://doi.org/10.1016/j.modpat.2024.100444

Pipitone, R. M., Ciccioli, C., Infantino, G., La Mantia, C., Parisi, S., Tulone, A., Pennisi, G., Grimaudo, S., & Petta, S. (2023). MAFLD: A multisystem disease. *Therapeutic Advances in Endocrinology and Metabolism*, *14*, 20420188221145549. https://doi.org/10.1177/20420188221145549

Pirmoazen, A. M., Khurana, A., El Kaffas, A., & Kamaya, A. (2020). Quantitative ultrasound approaches for diagnosis and monitoring hepatic steatosis in nonalcoholic fatty liver disease. *Theranostics*, *10*(9), 4277–4289. https://doi.org/10.7150/thno.40249

Postic, C., & Magnuson, M. A. (2000). DNA excision in liver by an albumin-Cre transgene occurs progressively with age. *Genesis*, *26*(2), 149–150. https://doi.org/10.1002/(SICI)1526-968X(200002)26:2%253C149::AID-GENE16%253E3.0.CO;2-V

Postic, C., Shiota, M., Niswender, K. D., Jetton, T. L., Chen, Y., Moates, J. M., Shelton, K. D., Lindner, J., Cherrington, A. D., & Magnuson, M. A. (1999). Dual Roles for Glucokinase in Glucose Homeostasis as Determined by Liver and Pancreatic β Cell-specific Gene Knock-outs Using Cre Recombinase. *Journal of Biological Chemistry*, *274*(1), 305–315. https://doi.org/10.1074/jbc.274.1.305

Poutanen, M., Miettinen, M., & Vihko, R. (1993). Differential estrogen substrate specificities for transiently expressed human placental 17 beta-hydroxysteroid dehydrogenase and an endogenous enzyme expressed in cultured COS-m6 cells. *Endocrinology*, *133*(6), 2639–2644. https://doi.org/10.1210/endo.133.6.8243287

Qidwai, K., Afkhami, M., & Day, C. E. (2014). The Pathologist's Guide to Fixatives. In C. E. Day (Ed.), *Histopathology* (Vol. 1180, pp. 21–30). Springer New York. https://doi.org/10.1007/978-1-4939-1050-2_2

Ramot, Y., Deshpande, A., Morello, V., Michieli, P., Shlomov, T., & Nyska, A. (2021). Microscope-Based Automated Quantification of Liver Fibrosis in Mice Using a Deep Learning Algorithm. *Toxicologic Pathology*, *49*(5), 1126–1133. https://doi.org/10.1177/01926233211003866

Ramot, Y., Zandani, G., Madar, Z., Deshmukh, S., & Nyska, A. (2020). Utilization of a Deep Learning Algorithm for Microscope-Based Fatty Vacuole Quantification in a Fatty Liver Model in Mice. *Toxicologic Pathology*, *48*(5), 702–707. https://doi.org/10.1177/0192623320926478

Rantakari, P., Lagerbohm, H., Kaimainen, M., Suomela, J. P., Strauss, L., Sainio, K., Pakarinen, P., & Poutanen, M. (2010). Hydroxysteroid (17{beta}) dehydrogenase 12 is essential for mouse organogenesis and embryonic survival. *Endocrinology*, *151*(4), 1893–1901. https://doi.org/10.1210/en.2009-0929

Reimer, L., & Kohl, H. (2008). *Transmission electron microscopy: Physics of image formation* (5th ed). Springer.

Rinella, M. E., Lazarus, J. V., Ratziu, V., Francque, S. M., Sanyal, A. J., Kanwal, F., Romero, D., Abdelmalek, M. F., Anstee, Q. M., Arab, J. P., Arrese, M., Bataller, R., Beuers, U., Boursier, J., Bugianesi, E., Byrne, C. D., Castro Narro, G. E., Chowdhury, A., Cortez-Pinto, H., … Newsome, P. N. (2023). A multisociety Delphi consensus statement on new fatty liver disease nomenclature. *Journal of Hepatology*, *79*(6), 1542–1556. https://doi.org/10.1016/j.jhep.2023.06.003

Río, L. A. del. (2013). *Peroxisomes and their key role in cellular signaling and metabolism*. Springer.

Rogers, A. B., & Dintzis, R. Z. (2012). 13—Liver and Gallbladder. *Comparative Anatomy and Histology*, *Generic*, 193–201. https://doi.org/10.1016/B978-0-12-381361-9.00013-5

Roy, M., Wang, F., Vo, H., Teng, D., Teodoro, G., Farris, A. B., Castillo-Leon, E., Vos, M. B., & Kong, J. (2020). Deep-learning-based accurate hepatic steatosis quantification for histological assessment of liver biopsies. *Laboratory Investigation; a Journal of Technical Methods and Pathology*, *100*(10), 1367–1383. https://doi.org/10.1038/s41374-020-0463-y

Rozga, J. (2002). Hepatocyte proliferation in health and in liver failure. *Medical Science Monitor: International Medical Journal of Experimental and Clinical Research*, *8*(2), RA32-38.

Ruifrok, A. C., & Johnston, D. A. (2001). Quantification of histochemical staining by color deconvolution. *Analytical and Quantitative Cytology and Histology*, *23*(4), 291–299.

Russell, W. M. S., & Burch, R. L. (with Universities Federation for Animal Welfare). (1992). *The principles of humane experimental technique* (Special ed., [Nachdr. der Ausg.] London 1959). Universities Federation for Animal Welfare.

Ruusuvuori, P., Valkonen, M., Kartasalo, K., Valkonen, M., Visakorpi, T., Nykter, M., & Latonen, L. (2022). Spatial analysis of histology in 3D: Quantification and visualization of organ and tumor level tissue environment. *Heliyon*, *8*(1), e08762. https://doi.org/10.1016/j.heliyon.2022.e08762

Sakurai, N., Miki, Y., Suzuki, T., Watanabe, K., Narita, T., Ando, K., Yung, T. M. C., Aoki, D., Sasano, H., & Handa, H. (2006). Systemic distribution and tissue localizations of human 17beta-hydroxysteroid dehydrogenase type 12. *The Journal of Steroid Biochemistry and Molecular Biology*, *99*(4–5), 174–181. https://doi.org/10.1016/j.jsbmb.2006.01.010

Saloniemi, T., Jokela, H., Strauss, L., Pakarinen, P., & Poutanen, M. (2012). The diversity of sex steroid action: Novel functions of hydroxysteroid (17β) dehydrogenases as revealed by genetically modified mouse models. *Journal of Endocrinology*, *212*(1), 27–40. https://doi.org/10.1530/JOE-11-0315

Schindelin, J., Arganda-Carreras, I., Frise, E., Kaynig, V., Longair, M., Pietzsch, T., Preibisch, S., Rueden, C., Saalfeld, S., Schmid, B., Tinevez, J.-Y., White, D. J., Hartenstein, V., Eliceiri, K., Tomancak, P., & Cardona, A. (2012). Fiji: An open-source platform for biological-image analysis. *Nature Methods*, *9*(7), 676–682. https://doi.org/10.1038/nmeth.2019

Schwartz, R., Dodge, J., Smith, N. A., & Etzioni, O. (2019). *Green AI* (Version 3). arXiv. https://doi.org/10.48550/ARXIV.1907.10597

Schwen, L. O., Homeyer, A., Schwier, M., Dahmen, U., Dirsch, O., Schenk, A., Kuepfer, L., Preusser, T., & Schenk, A. (2016). Zonated quantification of steatosis in an entire mouse liver. *Computers in Biology and Medicine*, *73*, 108–118. https://doi.org/10.1016/j.compbiomed.2016.04.004

Serdjebi, C., Bertotti, K., Huang, P., Wei, G., Skelton-Badlani, D., Leclercq, I. A., Barbes, D., Lepoivre, B., Popov, Y. V., & Julé, Y. (2022). Automated whole slide image analysis for a translational quantification of liver fibrosis. *Scientific Reports*, *12*(1), 17935. https://doi.org/10.1038/s41598-022-22902-w

Sethunath, D., Morusu, S., Tuceryan, M., Cummings, O. W., Zhang, H., Yin, X.-M., Vanderbeck, S., Chalasani, N., & Gawrieh, S. (2018). Automated assessment of steatosis in murine fatty liver. *PLOS ONE*, *13*(5), e0197242. https://doi.org/10.1371/journal.pone.0197242

Shen, Y., Luo, Y., Shen, D., & Ke, J. (2022). *RandStainNA: Learning Stain-Agnostic Features from Histology Slides by Bridging Stain Augmentation and Normalization*. https://doi.org/10.48550/ARXIV.2206.12694

Sherman, B. T., Hao, M., Qiu, J., Jiao, X., Baseler, M. W., Lane, H. C., Imamichi, T., & Chang, W. (2022). DAVID: A web server for functional enrichment analysis and functional annotation of gene lists (2021 update). *Nucleic Acids Research*, *50*(W1), W216–W221. https://doi.org/10.1093/nar/gkac194

Song, N.-J., Kim, S., Jang, B.-H., Chang, S.-H., Yun, U. J., Park, K.-M., Waki, H., Li, D. Y., Tontonoz, P., & Park, K. W. (2016). Small Molecule-Induced Complement Factor D (Adipsin) Promotes

Lipid Accumulation and Adipocyte Differentiation. *PLOS ONE*, *11*(9), e0162228. https://doi.org/10.1371/journal.pone.0162228

Sriboonaied, P., Phuangbubpha, P., Saetan, P., Charoensuksai, P., & Charoenpanich, A. (2025). Dual Modulation of Adipogenesis and Apoptosis by PPARG Agonist Rosiglitazone and Antagonist Betulinic Acid in 3T3-L1 Cells. *Biomedicines*, *13*(6), 1340. https://doi.org/10.3390/biomedicines13061340

Stacke, K., Eilertsen, G., Unger, J., & Lundstrom, C. (2021). Measuring Domain Shift for Deep Learning in Histopathology. *IEEE Journal of Biomedical and Health Informatics*, *25*(2), 325–336. https://doi.org/10.1109/JBHI.2020.3032060

Strubell, E., Ganesh, A., & McCallum, A. (2019). *Energy and Policy Considerations for Deep Learning in NLP* (Version 1). arXiv. https://doi.org/10.48550/ARXIV.1906.02243

Su, W., Wu, S., Yang, Y., Guo, Y., Zhang, H., Su, J., Chen, L., Mao, Z., Lan, R., Cao, R., Wang, C., Xu, H., Zhang, C., Li, S., Gao, M., Chen, X., Zheng, Z., Wang, B., Liu, Y., … Guan, Y. (2022). Phosphorylation of 17β-hydroxysteroid dehydrogenase 13 at serine 33 attenuates nonalcoholic fatty liver disease in mice. *Nature Communications*, *13*(1), 6577. https://doi.org/10.1038/s41467-022-34299-1

Suchy, F. J., Boron, W. F., & Boulpaep, E. L. (Eds.). (2017). Hepatobiliary function. In *Medical physiology* (Third Edition, pp. 944–971). Elsevier.

Taqi, S. A., Sami, S. A., Sami, L. B., & Zaki, S. A. (2018). A review of artifacts in histopathology. *Journal of Oral and Maxillofacial Pathology: JOMFP*, *22*(2), 279. https://doi.org/10.4103/jomfp.JOMFP_125_15

Targher, G., Byrne, C. D., & Tilg, H. (2024). MASLD: A systemic metabolic disorder with cardiovascular and malignant complications. *Gut*, gutjnl-2023-330595. https://doi.org/10.1136/gutjnl-2023-330595

Taylor, C. R. (2014). Immunohistochemistry in Surgical Pathology: Principles and Practice. In C. E. Day (Ed.), *Histopathology* (Vol. 1180, pp. 81–109). Springer New York. https://doi.org/10.1007/978-1-4939-1050-2_5

Taylor, C. R., & Levenson, R. M. (2006). Quantification of immunohistochemistry—Issues concerning methods, utility and semiquantitative assessment II. *Histopathology*, *49*(4), 411–424. https://doi.org/10.1111/j.1365-2559.2006.02513.x

Trefts, E., Gannon, M., & Wasserman, D. H. (2017). The liver. *Current Biology*, *27*(21), R1147–R1151. https://doi.org/10.1016/j.cub.2017.09.019

Tsachaki, M., & Odermatt, A. (2019). Subcellular localization and membrane topology of 17beta-hydroxysteroid dehydrogenases. *Molecular and Cellular Endocrinology*, *489*(Journal Article), 98–106.

Tsuru, H., Osaka, M., Hiraoka, Y., & Yoshida, M. (2020). HFD-induced hepatic lipid accumulation and inflammation are decreased in Factor D deficient mouse. *Scientific Reports*, *10*(1), 17593. https://doi.org/10.1038/s41598-020-74617-5

Tweel, J. E. D., Ecclestone, B. R., Boktor, M., Dinakaran, D., Mackey, J. R., & Reza, P. H. (2023). *Automated Whole Slide Imaging for Label-Free Histology using Photon Absorption Remote Sensing Microscopy* (Version 2). arXiv. https://doi.org/10.48550/ARXIV.2304.13736

Walker, R. A. (2006). Quantification of immunohistochemistry—Issues concerning methods, utility and semiquantitative assessment I. *Histopathology*, *49*(4), 406–410. https://doi.org/10.1111/j.1365-2559.2006.02514.x

Wang, G., Zhao, D., Spring, D. J., & DePinho, R. A. (2018). Genetics and biology of prostate cancer. *Genes & Development*, *32*(17–18), 1105–1140. https://doi.org/10.1101/gad.315739.118

Wang, M., Li, J., Li, H., Dong, B., Jiang, J., Liu, N., Tan, J., Wang, X., Lei, L., Li, H., Sun, H., Tang, M., Wang, H., Yan, H., Li, Y., Jiang, J., & Peng, Z. (2022). Down-Regulating the High Level of 17-Beta-Hydroxysteroid Dehydrogenase 13 Plays a Therapeutic Role for Non-Alcoholic Fatty Liver Disease. *International Journal of Molecular Sciences*, *23*(10), 5544. https://doi.org/10.3390/ijms23105544

Weisend, C. M., Kundert, J. A., Suvorova, E. S., Prigge, J. R., & Schmidt, E. E. (2009). Cre activity in fetal *albCre* mouse hepatocytes: Utility for developmental studies. *Genesis*, *47*(12), 789–792. https://doi.org/10.1002/dvg.20568

Xu, R., Pan, J., Zhou, W., Ji, G., & Dang, Y. (2022). Recent advances in lean NAFLD. *Biomedicine & Pharmacotherapy*, *153*, 113331. https://doi.org/10.1016/j.biopha.2022.113331

Yan, Y., Yang, N., Qin, F., & Hao, Y. (2024). Echinacoside Alleviates Metabolic Dysfunction-Associated Steatotic Liver Disease by Inhibiting Ferroptosis via Nrf2/HMOX1 Pathway. *Biomedicines*, *12*(12), 2728. https://doi.org/10.3390/biomedicines12122728

Younossi, Z. M., Golabi, P., Paik, J. M., Henry, A., Van Dongen, C., & Henry, L. (2023). The global epidemiology of nonalcoholic fatty liver disease (NAFLD) and nonalcoholic steatohepatitis (NASH): A systematic review. *Hepatology*, *77*(4), 1335–1347. https://doi.org/10.1097/HEP.0000000000000004

Younossi, Z. M., & Henry, L. (2024). Understanding the Burden of Nonalcoholic Fatty Liver Disease: Time for Action. *Diabetes Spectrum*, *37*(1), 9–19. https://doi.org/10.2337/dsi23-0010

Younossi, Z. M., Wong, G., Anstee, Q. M., & Henry, L. (2023). The Global Burden of Liver Disease. *Clinical Gastroenterology and Hepatology*, *21*(8), 1978–1991. https://doi.org/10.1016/j.cgh.2023.04.015

Yu, Y., Wang, J., Ng, C. W., Ma, Y., Mo, S., Fong, E. L. S., Xing, J., Song, Z., Xie, Y., Si, K., Wee, A., Welsch, R. E., So, P. T. C., & Yu, H. (2018). Deep learning enables automated scoring of liver fibrosis stages. *Scientific Reports*, *8*(1), 16016. https://doi.org/10.1038/s41598-018-34300-2

Zadoorian, A., Du, X., & Yang, H. (2023). Lipid droplet biogenesis and functions in health and disease. *Nature Reviews Endocrinology*, *19*(8), 443–459. https://doi.org/10.1038/s41574-023-00845-0

Zhang, N., Sheng, M., Wu, M., Zhang, X., Ding, Y., Lin, Y., Yu, W., Wang, S., & Du, H. (2019). Berberine protects steatotic donor undergoing liver transplantation via inhibiting endoplasmic reticulum stress-mediated reticulophagy. *Experimental Biology and Medicine*, *244*(18), 1695–1704. https://doi.org/10.1177/1535370219878651

Zheng, Y. (2023). 274-LB: Complement Factor D Contributes to Metabolic Dysregulation by Hepatic CD9 Deficiency. *Diabetes*, *72*(Supplement_1), 274-LB. https://doi.org/10.2337/db23-274-LB

List of Figures and Tables

Figures

Tables

TURUN
YLIOPISTO
UNIVERSITY
OF TURKU

Painosalama, Turku, Finland 2025

ISBN 978-952-02-0473-0 (PRINT)
ISBN 978-952-02-0474-7 (PDF)
ISSN 0355-9483 (Print)
ISSN 2343-3213 (Online)